# Heavy Elastica soil-supported with lifting load and bending moment applied to an end: A new analytical approach for very large displacements and experimental validation

Christian Iandiorio, Pietro Salvini

# Heavy Elastica soil-supported with lifting load and bending moment applied to an end: a new analytical approach for very large displacements and experimental validation

**Authors:** Christian Iandiorio - c.iandiorio@live.it
Pietro Salvini - salvini@uniroma2.it
Corresponding Author: salvini@uniroma2.it

**Affiliations:** Department of Enterprise Engineering
University of Rome "Tor Vergata",
Via del Politecnico 1, 00133 Rome, EU,
Italy

---

**Abstract.** The Heavy Elastica problem is a classical issue and has been addressed by many authors. The only analytical approach applied is the perturbative method, and the expansion through Taylor's series is the most recurrent technique. This transforms the nonlinear differential problem into a system of nonlinear (trigonometric) algebraic equations to compute the expansion coefficients. The main disadvantage is that the size of the obtained nonlinear systems is equal to the degree of the series expansion of the solution; therefore, to gain a good accuracy, it is necessary to manage the series expansion up to a considerable degree. Possibly for this reason, the use of perturbative techniques has gradually been abandoned and many authors have addressed the problem of Heavy Elastica with numerical methods. In this paper, a new analytical method based on the parabolic curvilinear abscissa mapping is presented. The result is that the problem of the Heavy Elastica takes on the same complexity as the well-known Elastica problem (concentrated forces and moment applied) and is therefore solved. The proposed method is compared with the

Runge-Kutta integration approach and finite element results, showing the correctness of the solution suggested and its remarkable computational advantage. A further comparison is carried out by means of a number of experimental tests that agree with the analytical expected values. By expressing the proposed solution in a dimensionless form, Design Charts are given; they provide the results in the whole field of the domain, so that both kinematic and static variables can be deduced without computer aid.

**Keywords.** Heavy Elastica; Large displacements and rotations;
Analytical method; Soil supported; Experimental validation

---

## Nomenclature

| | |
|---|---|
| $A$ | section area |
| $E$ | longitudinal modulus of elasticity |
| $F$ | lifting load |
| $g$ | gravitational acceleration |
| $I$ | moment of inertia |
| $k$ | curvature of the beam reference line (elastic curve) |
| $L$ | inflection length |
| $L_{tot}$ | total beam length |
| $M$ | lifting bending moment |
| $q$ | distributed load |
| $R$ | contact force |
| $s$ | curvilinear abscissa |
| T | shear force |
| U | strain potential energy |
| W | load potential energy |
| $x$ | abscissa coordinate of the Cartesian reference |
| $x_L$ | Cartesian abscissa coordinate at the lifting point |
| $y$ | ordinate coordinate of the cartesian reference |
| $y_L$ | Cartesian ordinate coordinate at the lifting point |
| $\varepsilon$ | stretch strain |
| $\xi$ | total potential energy |
| $\rho$ | mass density |
| $\sigma$ | component of the stress tensor associated at the tangent unit vector |
| $\boldsymbol{\tau}$ | unit tangent vector |
| $\psi$ | angle between the unit tangent vector and the Cartesian abscissa |
| $\psi_L$ | value of angle $\psi$ at the lifting point |

# 1 Introduction

Contact mechanics is a fundamental branch of solids and structural mechanics. It has many applications in engineering problems, as contact between balls and fifth wheel in plain bearings, matching of teeth in gear wheels, interaction between rail and locomotives wheels, in braking and friction systems and many others. In several of these applications the bodies in contact have curved edge surfaces. This implies that when two deformable bodies are pressed each other, the contact zone can be considered small if compared to the characteristic dimensions of the bodies (curvature radii). In these cases, the study of the deformed shape (kinematics) of the non-contacting portion of the bodies is marginal; the focus is the stress state close to contact area, which is three-dimensional. This implies an approach that makes full use of three-dimensional solid mechanics. The applications above described do not represent all cases of interest; there is a class of problems in which the deformed configuration is fundamental to derive the contact area and eventually its local stress field. An example is the smooth contact problem of a semi-infinite elastic layer, subjected to own weight, on a rigid foundation. The problem is addressed by Keer and Silva (1972), who provide an analytical solution using the Fredholm integral equations, assuming infinitesimal field of strain, displacements and rotations. A simpler discussion of this problem, using the beam theory, is given by Feodosyev (1977). Keer and Silva highlighted that this case is analogous to a crack (mode I) in a semi-infinite layer. It is indeed the refined version of the first analytical models to measure the splitting strength of polished plane surfaces, early discussed by Obreimoff (1930). His method, demonstrated for mica, can be applied to other fragile and flaking materials. This is a classical problem discussed in many influential books (Landau and Lifšits 1963; Wnuk 1990; Popov 2017; Barber 2018). In the paper of Keer and Silva (1972) and again in Kim et al. (2014), the size of the contact area is of the same order of the thickness of the beam. The contact area is defined as the distance between the first contact region and the zone where the stress distribution returns to its nominal value.

A broad field of research on the Elastica concerns the adhesion problem, as the lifting with adhesion (O'Reilly 2017 reports an extensive literature) and the stability of adhesive states between an Elastica and a rigid halfspace (Majidi et al 2012). Adhesion effects, as introduced in these last papers, are not considered in our developments since the soil contact does not provide any considerable adhesive effect.

The present paper investigates the behaviour of a weighting beam (one dimensional problem) loaded at one end with concentrated vertical load and bending moment on a rigid foundation. There are no restrictions on the deformed (i.e. final or current) configuration, so that finite displacements and rotations occur. However, strain field is assumed infinitesimal and shear strains have a negligible influence; this implies that the finite rotation of the section is assumed as only due to bending. This allows imputing the cause of the nonlinearity only to the geometric shape modification of the beam axis. It is straightforward that this behaviour covers slender structures or, more specifically, thin beams.

For rectangular sections, hereinafter considered, this occurs when the beam height is so small and strains results limited even if the overall assumed curvature is considerable. In other words, the material response lies within the elastic behaviour. In such a case, the section inertia moments keeps almost the same value weather the beam is unloaded or loaded. Furthermore, for such thin beams, the energetic contribution of axial load is several orders of magnitude lower than the bending one; so that, it is straightforward to consider the beam length preservation when the loading configuration results in a considerable change of curvature. This beam configuration loading, where there are no limitations on displacements and rotations amounts, is commonly called Bernoulli-Euler *Elastica*.

When distributed loads are also present, e.g. own weight, the loading problem is addressed as *Heavy Elastica.* The unilateral contact problem of *Heavy Elastica* is addressed in Solyaev et al. (2019). The thickness of the beam is small so that it is suitable modelling a contact problem with a one-dimensional approach. Solyaev et al. (2019) face the problem through a classic perturbative approach inasmuch the differential government equation is nonlinear and not manageable by well-known solutions. The perturbative approach was applied for the first time in the case of the

*Heavy Elastica* by Rohde (1953) and it is widely discussed by Frish-Fay (1962). The method consists in expanding the unknown kinematic variable (slope angle) by a power series of the curvilinear abscissa (Taylor expansion); this is the most used approach by many authors for an analytical solution of the *Heavy Elastica*. A similar approach has been used by Schmidt and DaDeppo (1970) to study the *Heavy Elastica Column*, i.e. the post-buckling deflection of a beam-column. Considering cantilever beams, the same authors Schmidt and DaDeppo (1971) use a series expansion of trigonometric terms involving the ordinary Bessel functions and Chebyshev polynomials. Considering only the $\mathsf{zero}^{\mathsf{th}}$ and first-order Chebyshev polynomials they obtain a linearization of the governing equation which looks like a quasi-linear differential equation. However, their solution is accurate only for moderate displacements and rotations. Another interesting variation of the perturbation method is employed in another work by DaDeppo and Schmidt (1971) where the authors transform the nonlinear differential equation into a system of linear differential equations. Typically, the perturbation approach involves that the solution of the nonlinear differential equation is transformed into a solution of a system of nonlinear equations or of a system of linear differential equations. The major disadvantage is that the size of the resulting systems is equal to the degree of the series expansion considered. A consistent number of terms is required to obtain a good accuracy. Therefore, the resolving system must grows in complexity if the final displacements are consistent. This involves the computer aid trough numerical algorithms. None of the authors so far mentioned, has ever shown the convergence of the series expansion. This was first done in Wang (1981), and further discussed in Wang (1986), where the author pointed out that the power series expansion in curvilinear abscissa does not guarantee the converges at the boundary $s = L$. He also showed that the series diverges for high value of the dimensionless parameter $\frac{qL}{EI}$. To avoid this problem, recent numerical applications of the perturbation theory concern the use of the Homotopy Analysis Method (HAM) (Xiao 2011; Kimiaeifar et al. 2014; Maleki et al. 2014). Its main advantage is the control of the series convergence during the coefficients computation. This method necessarily requires the use of Symbolic Computer Algebra.

The Heavy Elastica problem has also been addressed with full numerical methods, as the finite difference method in Wang et al. (1961) or by Runge-Kutta integration method, as in Holden (1972). Another way to approach the problem is giving up the search of the solution of the intrinsic differential equation, accounting the curvature in a Cartesian form (Fertis 2006; Chen 2010; Mingari Scarpello and Ritelli 2011; Ghuku and Saha 2016). Unfortunately, this approach requires a-priori knowledge of the bending moment with respect to the Cartesian abscissa, which cannot be written explicitly if the beam is subjected to a distributed load, inasmuch the bending moment is also a function of the curvilinear abscissa. These approaches is therefore recommended only for the case of moderate displacements and rotations.

The solution system herein proposed deduces the government equations by means of Euler Variational Principle of least effort[1].

For solving the Integro-Differential System (which presents a non-linear differential equation with non-constant coefficients), an original method that offers a new way of dealing with this type of problem is presented. The basic idea is to give up the search of an exact analytical solution, assuming a parabolic map between the curvilinear abscissa $s$ and the Cartesian abscissa $x$. This method will be called hereinafter *Curvilinear Abscissa Mapping Method*. The idea of setting a map between $s$ and $x$ has also been discussed in Fertis (2006) who chooses a linear relationship of the type $s\ x\ = x + \Delta$, where $\Delta$ is a constant value. This linear expression of $s\ x\ $ loses accuracy when displacements increase, as shown in §4. In the approach followed in this paper, the coefficients of the parabolic mapping are not derived by a series expansion, but by the imposition of the three intersection points of the parabola. Two of them are obvious (starting and ending points), while the intermediate point implies a free choice. Although, the variability given by this free choice is then suppressed with the introduction of a closing equation. In fact, this last involves

[1] Euler L. in *Reflexions sur quelques loix generales de la nature qui s'observent dans les effets des forces quelconques,* Mémoires de l'académie des sciences de Berlin 4, 1750, pp. 189-218, extended the Maupertuis Principle of least action (1746) for dynamic systems also to static systems. He defined as Principle of least effort what is also nowadays called Principle of least potential energy.

a problem variable, i.e. the angle between the unit tangent vector and the Cartesian abscissa at the end lifting point. Parabolic mapping allows to obtain an analytical solution in integral form, also valid for very large displacements and rotations. As a matter of fact, the heavy Elastica solution assumes a form that is similar to the commonly known solution of the Elastica (no own load). In §3 Design Charts are given, i.e. the graphs of the dimensionless equations which provide the loads, displacements and rotations variables for the physical range of existence. In §4.1 an example is shown in which the analytical solution obtained in § 2 is compared with the solution deduced by the Runge-Kutta integration method (explaining how to get it and why it cannot be applied on a single integration shot), and by finite element method. Furthermore, in the same example, the solution is shown with a simpler linear curvilinear abscissa mapping, to highlight an increasing spread with the expected results when large displacements and rotations occurs. In the same paragraph it is highlighted that the proposed method involves a considerable reduction in the computation time, if compared with other full numerical methods. Finally, in §4.2 experimental tests are shown and compared with above mentioned methods.

# 2 Mathematical Framework

## 2.1 Deduction of the government equations

The vector $\boldsymbol{r} = x\boldsymbol{e_1} + y\boldsymbol{e_2}$ gives the position of a point belonging to the curve in the deformed configuration of the Elastica. Fig.1 gives a view of the reference system adopted whose origin is located at the first contact point. The unit vectors $\boldsymbol{e_1} = (1,0,0)^T$, $\boldsymbol{e_2} = (0,1,0)^T$, $\boldsymbol{e_3} = (0,0,1)^T$ are the base vectors of the orthogonal Cartesian reference. The unit tangent vector is defined as:

$$\boldsymbol{\tau} = \frac{d\boldsymbol{r}}{ds} = \frac{dx}{ds}\boldsymbol{e_1} + \frac{dy}{ds}\boldsymbol{e_2} \tag{1}$$

Using the known relations:

$$cos\,\psi = \frac{\boldsymbol{\tau} \cdot \boldsymbol{e_1}}{||\boldsymbol{\tau}||\,||\boldsymbol{e_1}||} \tag{2}$$

$$sin\,\psi = \frac{||\boldsymbol{\tau} \times \boldsymbol{e_1}||}{||\boldsymbol{\tau}||\,||\boldsymbol{e_1}||} \tag{3}$$

One obtains two fundamental equations:

$$\frac{dx}{ds} = cos\,\psi \tag{4}$$

$$\frac{dy}{ds} = sin\,\psi \tag{5}$$

The curvature is defined as:

$$k(s) = \left\|\frac{d\boldsymbol{\tau}}{ds}\right\| = \frac{d\psi}{ds} \tag{6}$$

These exhaust the set of necessary equations for the intrinsic geometry approach to plane curves. To deduce the equilibrium equation, the Euler's Least Effort Principle is used. It asserts that a system of bodies in equilibrium assumes the state that minimizes the total potential energy:

$$\xi = U - W \tag{7}$$

Where the classic signs convention of the first Principle of Thermodynamics is used. Assuming the one-dimensional beam model implies that the shape of the section is always preserved. Furthermore, the stress-strain relationship keeps linear, the material is homogeneous and isotropic, the beam is initially straight (no unloaded curvature) and the shape of the section is the same along the beam axis.

It is straightforward to show that in the ratios between the potential energy of shear versus bending and axial deformation versus bending, the energy ratios appear both dependent on $\left(\frac{I}{A}\right)$. This last is proportional to the inverse of the squared Euler's slenderness factor. The beams that

allows a large deformation while remaining within the elastic behaviour of the material and keeping the section almost unchanged are generally "thin". Therefore the energy contributions due to shear and axial extension result of many orders smaller than the energy contribution due to bending alone. This implies that in our modelling the bending strain is the only accounted energy contribution; according to this assumption, the length of the beam is preserved.

Models that consider the effects neglected here to deduce the governing equations are available in Reissner (1972) and Antman (1995). However, these approaches introduce mathematical complications that increase the difficulties in the search of analytical solutions which are non-balanced by a significant shift of the expected results.

Using (6) and the known relationship between the strain and curvature one obtains:

$$U(s) = \int_L \int_A \int_0^{\varepsilon} \sigma(\varepsilon)\, d\varepsilon\, dA\, ds = \int_L \frac{EI}{2} (\psi')^2 ds \tag{8}$$

Where the apex indicates the derivative by respect to the curvilinear abscissa $s$. The load potential energy is the sum of the potential energy of the distributed load $q$, of the end-load $F$ and of the end-moment $M$:

$$W = W_q + W_F + W_M \tag{9}$$

where:

$$W_q = \int_0^{y_L} q(L-s)\ (-\boldsymbol{e_2}) \cdot \boldsymbol{e_2}\, dy = -\int_0^{L} q(L-s)\ sin\,\psi\, ds \tag{10}$$

$$W_F = F\, y_L\, \boldsymbol{e_2} \cdot \boldsymbol{e_2} = \int_0^{L} F\, sin\,\psi\, ds \tag{11}$$

$$W_M = M\, \psi_L\, \boldsymbol{e_3} \cdot \boldsymbol{e_3} = \int_0^{L} M\, \psi'\, ds \tag{12}$$

In the (10),(11) it is assumed that the positive direction of $q$ and $F$ are in the y-direction and (12) includes the assumption $M(s=0)=0$.

The Euler's Least Effort Principle implies, when equilibrium is reached, that the first variation of the total potential energy is zero:

$$\delta\xi = \delta U - \delta W = 0 \tag{13}$$

Assuming the density of potential energies $u, w, w_q, w_F, w_M$, using the linearity of the variational operator $\delta$ and integrating by parts:

$$\delta U = \int_0^L \delta u(s,\psi')ds = \int_0^L \frac{\partial u}{\partial \psi'}\,\delta\psi'\,ds = \int_0^L EI\,\psi'\,(\delta\psi)'\,ds = [EI\,\psi'\,\delta\psi]\Big|_0^L - \int_0^L EI\;\psi''\,\delta\psi\,ds \tag{14}$$

$$\delta W_q = \int_0^L \delta w_q(s,\psi)\,ds = \int_0^L \frac{\partial w_q}{\partial \psi}\,\delta\psi\,ds = -\int_0^L q(L-s)\cos\psi\,\delta\psi\,ds \tag{15}$$

$$\delta W_F = \int_0^L \delta w_F(s,\psi)\,ds = \int_0^L \frac{\partial w_F}{\partial \psi}\,\delta\psi\,ds = \int_0^L F\cos\psi\,\delta\psi\,ds \tag{16}$$

$$\delta W_M = \int_0^L \delta w_M(s,\psi')ds = \int_0^L \frac{\partial w_M}{\partial \psi'}\,\delta\psi'\,ds = [M\,\delta\psi]\Big|_{\mathrm{L}} \tag{17}$$

Summing the previous contributions:

$$\delta W = [M\,\delta\psi]\Big|_0^L + \int_0^L [-q(L-s)+F]\cos\psi\,\delta\psi\,ds \tag{18}$$

Using eq. (13), (14) and (17):

$$[(EI\,\psi' - M)\,\delta\psi]\Big|_{s=L} - [EI\,\psi'\,\delta\psi]\Big|_{s=0} - [M\,\delta\psi]\Big|_{s=0} +$$

$$-\int_0^L \{EI\,\psi'' + [F - q(L-s)]cos\,\psi\}\delta\psi\,ds = 0 \tag{19}$$

Applying the fundamental Lemma of Variational Calculus, the governing non-linear differential equation results:

$$\psi'' + \frac{F - q(L-s)}{EI}\,cos\,\psi = 0 \tag{20}$$

with the following boundary conditions:

$$\psi'\Big|_{s=L} = \frac{M}{EI} \tag{21}$$

$$\psi'\Big|_{s=0} = 0 \tag{22}$$

The equations of interest have now been deduced. It is important to highlight that the length $L$ is an unknown of the problem; this aspect will be discussed in detail in the next paragraph.

## 2.2 Application of the curvilinear abscissa mapping method

The complete set of equations governing the problem of the smooth unilateral contact of Heavy Elastica, with one-end lift without inflection point, includes the equations (20), the eq. resulting to inserting (4) into (5) and that due to the integration of (7):

$$\frac{d^2\psi(s)}{ds^2} + \frac{F - q(L-s)}{EI}\,cos\,\psi(s) = 0 \tag{23}$$

$$y(x) = y_0 + \int_0^x tan\;\psi\,d\tilde{x} \tag{24}$$

$$L = \int_0^{x_L} \frac{dx}{cos\,\psi} \tag{25}$$

and the following five boundary conditions:

$$\left.\frac{d\psi(s)}{ds}\right|_{s=L} = \frac{M}{EI} \tag{26}$$

$$\left.\frac{d\psi(s)}{ds}\right|_{s=0} = 0 \tag{27}$$

$$\left.\psi(s)\right|_{s=L} = \psi_L \tag{28}$$

$$\left.\psi(s)\right|_{s=0} = 0 \tag{29}$$

$$\left.y(x)\right|_{x=0} = y_0 = 0 \tag{30}$$

Where $\tilde{x}$ is a dummy integration variable. Note that the functions in (24) and (25) are never improper inasmuch the angle $\psi$ is bounded in the region $\psi \in \left[0, \frac{\pi}{2}\right)$.

These equations form a system of Integral-Differential-Equations (IDE) with mixed boundary condition. The eq.(23) is a second order, nonlinear, homogeneous, with non-constant coefficient differential equation. The eq. (24) is the equation giving the displaced configuration of the beam. It is lawful only if $\psi(s) \in \left(-\frac{\pi}{2}, \frac{\pi}{2}\right)$, but for the problem here discussed $\psi(s) \in \left[0, \frac{\pi}{2}\right)$. The eq. (25) states the length preservation. The boundary conditions are mixed Neumann and Dirichlet conditions, while the eq.s (28),(29) are an additional boundary condition. They do not derive from the Variational Principle, as they arise arising from the geometry (not mechanics) of the problem. As discussed below, (28) is an essential condition for the application of the curvilinear abscissa mapping method, but it is important to emphasize that $\psi_L$ is an unknown variable. It is fundamental to highlight that the inflection length $L$ is itself an unknown variable. This implies that it is not possible to directly apply a numerical procedure if not affected by an attempt method. This statement will be discussed in depth in §3.

The concentrated bending moment $M$ is counter-clockwise so that $\psi'(s = L) = \frac{M}{EI} > 0$. Being also $\psi'(s = 0) = 0$ , $\psi(s = 0) = 0$ and $\psi_L(s = L) > 0$ it follows that $\psi(s)$ is a monotonically increasing function, i.e. there are no inflection points. This is to say that the curvature cannot assume a zero value at every internal point. On the contrary, if the ending $M$ is clockwise, namely

$\psi'(s = L) = \frac{M}{EI} < 0$, an inflection point does always occur. In such a case the curvilinear abscissa mapping method can still be actually used to solve the problem, but this case opens to a complex discussion that worth a dedicated paper.

The eq. (23) does not allow an exact analytical solution. The curvilinear abscissa mapping method hereinafter proposed, assuming a-priori map between the curvilinear abscissa and the Cartesian abscissa, provides an analytical solution of (23). Fertis (2006) proposed a linear mapping: $s(x) = x + \Delta$ where $\Delta = constant$; it is straightforward that this linear map does not respect the condition $s(x = 0) = 0$. This choice is not efficient for large rotations (and displacements) and is more suitable for moderate rotations. In this paper a parabolic mapping is assumed:

$$s(x) = \tilde{a} + \tilde{b}\, x + \tilde{c}\, x^2 \tag{31}$$

It is important to emphasize that the coefficients $\tilde{a}, \tilde{b}, \tilde{c}$ do not derive from a series expansion. The choice of a polynomial mapping is not the only possible strategy, but it gives advantage for the algebraic and integrate operations that follow. Moreover, it is important to highlight that this map is reversible; this is a profitable feature, as will be shown below. The intersection points of the parabolic map are of course imposed on the extreme ends, but an additional internal point is needed:

$$\begin{aligned} s = 0 \;&\mapsto\; x = 0 \\ s = L \;&\mapsto\; x = x_L \\ s = n\,L \;&\mapsto\; x = m\,L \end{aligned} \tag{32}$$

where $n, m \in (0,1)$. Imposing the conditions (32), the coefficients of the parabolic mapping are obtained as a function of $n$ and $m$:

$$\begin{aligned} \tilde{a} &= 0 \\ \tilde{b} &= \frac{L}{x_L}\,\frac{m^2 - n}{m\,(m-1)} \end{aligned} \tag{33}$$

$$\tilde{c} = \frac{L}{{x_L}^2} \frac{n-m}{m\,(m-1)}$$

The kinematic unknowns from which it is possible to derive all the other functions of interest are four: $\psi_L, x_L, y_L, L$. The equations that can be immediately used are only four, inasmuch eq.s (27) and (29) are used to determine two integration constants, while eq. (23) needs to be used in (24). This implies that $n$ and $m$ cannot be independent, but they must either be imposed a priori or be linked to one of the four kinematic unknowns. A suitable choice for $n$ is the middle value:

$$n = \frac{1}{2} \tag{34}$$

i.e. the third intersection point is equally distanced by the other two. An effective choice for $m$ is to assume $m = m(\psi_L)$. Being the last intersection point considered $s = \frac{L}{2}$ a rational choice is an interpolation with respect to the median angle $\frac{\psi_L}{2}$:

$$m(\psi_L) = \frac{n}{cos\left(\frac{\psi_L}{2}\right)} \tag{35}$$

This is not the only possible choice, but not all possible choices gives reliable results. The worth of a choice is measured by the ability to minimize the error in the assumption of a parabolic map of the curvilinear abscissa. The choice given by eq. (35) has proven to be very effective and reliable as shown through the comparisons with the results obtained through Runge-Kutta method, finite element discretization, and experimental evidences discussed in §4. The eq. (35) implies that for small $\psi_L$ values $m \to n$ obtaining $s(x) = \frac{L}{x_L}\, x$ i.e. for small displacements and rotations the mapping is linear, as resulting by first order solutions (linear theory). It is important to highlight that the form of the closure equation $m = m(\psi_L)$ does not modify in any way the resulting equations that will be obtained below. The procedure hereinafter discussed is indeed independent of the specific choice of $m$, provided that it is only function of $\psi_L$. Summarizing and compacting the notation:

$$s(\psi_L\ , u) = L\,(b\,u + c\,u^2) \tag{36}$$

where:

$$u = \frac{x}{x_L} \tag{37}$$

$$b(\psi_L) = \frac{m^2 - n}{m\,(m-1)} \tag{38}$$

$$c(\psi_L) = \frac{n - m}{m\,(m-1)} \tag{39}$$

Integrating once the equation (23) one obtains:

$$\frac{d\psi}{ds} = \int \frac{1}{EI}\,[q(L-s) - F]\,cos\,\psi\,ds + \,c_1 \tag{40}$$

where $c_1$ is an integration constant. Using the eq. (10) and the dimensionless $u$ defined in (37), it follows:

$$x_L\,\frac{du}{ds} = cos\,\psi \tag{41}$$

Applying (52) into (51):

$$\frac{d\psi}{ds} = \int \frac{1}{EI}\,[q(L-s) - F]\,x_L\,du + \,c_1 \tag{42}$$

So far, no approximation has been introduced. It is evident that the integral in (42) is not solvable. Applying the curvilinear abscissa parabolic mapping (36) in (42):

$$\frac{d\psi}{ds} = \int \frac{1}{EI}\,[qL(1 - b\,u - c\,u^2) - F]\,x_L\,du + \,c_1 \tag{43}$$

Now, in its actual form, the function in (43) can be easily integrated. Applying the b.c. (27) and considering that the point $s = 0$ corresponds to $x = 0$ and therefore $u = 0$, one obtains:

$$\frac{d\psi}{ds} = \frac{x_L\,u}{EI}\left[qL\left(1 - \frac{b}{2}\,u - \frac{c}{3}\,u^2\right) - F\right] \tag{44}$$

Using the b.c. (26) in (44), considering that the point $s = L$ corresponds to $x = x_L$ and $u = 1$:

$$\frac{M}{x_L} = qL\left(1 - \frac{b}{2} - \frac{c}{3}\right) - F \tag{45}$$

The eq. (45) will be used later on. Let us manipulate the eq. (44):

$$\frac{d\psi}{ds} = \frac{dx}{ds}\frac{du}{dx}\frac{d\psi}{du} = \frac{\cos\psi}{x_L}\frac{d\psi}{du} = \frac{x_L\, u}{EI}\left[qL\left(1 - \frac{b}{2}\,u - \frac{c}{3}\,u^2\right) - F\right] \tag{46}$$

Integrating the eq. (46) and using the b.c. (29) one obtain:

$$\sin\psi = \frac{{x_L}^2\, u^2}{2\,EI}\left[qL\left(1 - \frac{b}{3}\,u - \frac{c}{6}\,u^2\right) - F\right] \tag{47}$$

Applying the b.c. (28) on eq. (47):

$$\sin\psi_L = \frac{{x_L}^2}{2\,EI}\left[qL\left(1 - \frac{b}{3} - \frac{c}{6}\right) - F\right] \tag{48}$$

To simplify further equations, the following compact notation is introduced:

$$f_{a_1,a_2}(t) = 1 - \frac{b}{a_1}\,t - \frac{c}{a_2}\,t^2 \tag{49}$$

$with\ \ a_1, a_2 \in \mathbb{R}$.

Making use of notation (49), the equations (45) and (48) become:

$$\frac{M}{x_L} = qL\, f_{2,3}(1) - F \tag{50}$$

$$\sin\psi_L = \frac{{x_L}^2}{2\,EI}\left(qL\, f_{3,6}(1) - F\right) \tag{51}$$

Including eq. (50) into (51), and removing $qL$, one obtains:

$$2EI\ \sin\psi_L = {x_L}^2\left[\left(\frac{M}{x_L} + F\right)\frac{f_{3,6}(1)}{f_{2,3}(1)} - F\right] \tag{52}$$

Now two cases need to be distinguished: $M > 0$ and $M = 0$.

If $M > 0$, a second-degree equation in dimensionless form is obtained from the eq. (52):

$$\frac{F^2}{M^2}\left(\frac{1-f_{6,6}(1)}{f_{2,3}(1)}\right){x_L}^2+\frac{F}{M}\left(\frac{f_{3,6}(1)}{f_{2,3}(1)}\right)x_L-2\left(\frac{FEI}{M^2}\right)\sin\psi_L=0 \tag{53}$$

This equation provides the $x_L$ variable only as a function of $\psi_L$ and the known dimensionless parameter $\frac{FEI}{M^2}$. Note that the identity $f_{3,6}(1)-f_{2,3}(1)=1-f_{6,6}(1)$ has been used. Solving the second-degree equation (53):

$$x_L\left(\psi_L,\frac{FEI}{M^2}\right)=\frac{M}{F}f^* \tag{54}$$

where:

$$f^*\left(\psi_L,\frac{FEI}{M^2}\right)=\frac{1}{2}\left(\frac{f_{3.6}(1)}{1-f_{6,6}(1)}\right)\left[-1\pm\sqrt{1+8\left(\frac{FEI}{M^2}\right)\left(\frac{f_{2,3}(1)\left(1-f_{6,6}(1)\right)}{\left(f_{3,6}(1)\right)^2}\right)}\right] \tag{55}$$

Obviously, the solution of (55) preserving a physical meaning, has the positive sign.

If $M=0$, from the eq. (52) it derives a simple one order solution:

$$x_L(\psi_L)=\sqrt{\frac{EI}{F}}\sqrt{\frac{2\,f_{2,3}(1)\sin\psi_L}{1-f_{6,6}(1)}} \tag{56}$$

Appling the notation (49) the eq. (47) is expressed as:

$$\sin\psi\;=\frac{{x_L}^2\,u^2}{2\,EI}\;(qL\,f_{3.6}(u)-F) \tag{57}$$

Including eq. (50) into (57), removing $qL$, and using (52) to remove $x_L$ one obtains:

$$\sin\psi\;=\sin\psi_L\;u^2\;\frac{\left(\frac{M}{x_L}+F\right)\left(\frac{f_{3,6}(u)}{f_{2,3}(1)}\right)-F}{\left(\frac{M}{x_L}+F\right)\left(\frac{f_{3,6}(1)}{f_{2,3}(1)}\right)-F} \tag{58}$$

For the case of $M>0$, $x_L$ is given by (54) and substituted in (58):

$$\sin\psi\;\left(\psi_L,u,\frac{FEI}{M^2}\right)=\sin\psi_L\;u^2\;\frac{(1+f^*)\,f_{3,6}(u)-f^*\,f_{2,3}(1)}{(1+f^*)\,f_{3,6}(1)-f^*\,f_{2,3}(1)} \tag{59}$$

While for the $M = 0$ case, $x_L$ is given by (56) and substituted in (58):

$$\sin\psi\,(\psi_L, u) = \sin\psi_L\; u^2\; \frac{f_{3,6}(u) - f_{2,3}(1)}{1 - f_{6,6}(1)} \tag{60}$$

Appling the b.c. (30) and using the change of variable (37), the eq. (24) is expressed as:

$$y(u) = x_L \int_0^u \tan\psi\, d\tilde{u} = \int_0^u \frac{\sin\psi}{\sqrt{1 - sin^2\psi}}\, d\tilde{u} \tag{61}$$

For the case $M > 0$, using the eq.s (54) and (59) in (61) one obtains:

$$y(u) = \frac{M}{F}\, f^* \int_0^u \frac{\sin\psi}{\sqrt{1 - sin^2\,\psi}}\, d\tilde{u} \tag{62}$$

Where $\sin\psi$ function is expressed in (59). While for the case of $M = 0$, using the eq. (56) and (60) in (61) one has:

$$y(u) = \sqrt{\frac{EI}{F}} \sqrt{\frac{2\, f_{2,3}(1)\sin\psi_L}{1 - f_{6,6}(1)}} \int_0^u \frac{\sin\psi}{\sqrt{1 - sin^2\psi}}\, d\tilde{u} \tag{63}$$

Where $\sin\psi$ function, for this case, is expressed in (60). The integrals (62) and (63), when solved, allow the calculation of the full deformed configuration of the beam. These last integrals cannot be integrated analytically, therefore the use of the numerical calculation is required. However, we remark that so far, the only unknown variable is $\psi_L$. The last equation to be imposed is the length preservation (25). Applying again the change of variable (37) in the eq. (25):

$$\frac{L}{x_L} = \int_0^1 \frac{du}{\sqrt{1 - sin^2\psi}} \tag{64}$$

While from eq. (50):

$$L = \frac{1}{q\, f_{2,3}(1)} \left(\frac{M}{x_L} + F\right) \tag{65}$$

For the case of $M > 0$, using the eq. (54) in (65):

$$\frac{L}{x_L} = \frac{F^2}{Mq} \frac{1}{f^* f_{2,3}(1)} \left(1 + \frac{1}{f^*}\right) \tag{66}$$

Including the eq. (66) in (64):

$$\frac{F^2}{Mq} = \frac{f_{2,3}(1)\,(f^*)^2}{(1+f^*)} \int_0^1 \frac{du}{\sqrt{1-sin^2\psi}} \tag{67}$$

Where $\sin\psi$ function is expressed in (59).

For $M = 0$ case, instead, including eq. (65) in (64) and using the eq. (56) one obtains:

$$\frac{F^3}{q^2 EI} = \frac{2\left(f_{2,3}(1)\right)^3 sin\,\psi_L}{1 - f_{6,6}(1)} \left( \int_0^1 \frac{du}{\sqrt{1-sin^2\psi}} \right)^2 \tag{68}$$

Where $\sin\psi$ function, for this case, is referred to (60). The eq.s (67) and (68) are only functions of known dimensionless values and the angle $\psi_L$. These integrals cannot be solved analytically and require, as for (62) and (63), a numerical calculation. This is analogous to what is required in the case of classical Elastica, subjected to concentrated loads only. Hence, the obtained solution has the same complexity of the classical Elastica subject to end concentrated forces and moment only, Frish-Fay R. (1962).

It is straightforward to observe that according to the proposed method, the kinematic variables of a single point (e.g. the lifting point) avoids the integration on the entire length of the beam, as required by full numerical integration methods. Either from the eq. (67) or (68) one calculates the unknown variable $\psi_L$.

Considering $M > 0$ eq. (67) may be dependent of two dimensionless parameters $\frac{F^2}{Mq}$ and $\frac{FEI}{M^2}$, over the only variable $\psi_L$.

Considering $M = 0$ eq. (68) depends only of one dimensionless parameter $\frac{F^3}{q^2 EI}$.

The value of the variable $\psi_L$ through (67) or (69) needs to be obtained by an attempt method, limited to a single integral. This is not a consequence of the curvilinear abscissa mapping method.

This also happens in the case of the Elastica subjected to concentrated loads, e.g. cantilever beam (Frish-Fay 1962; Iandiorio and Salvini 2020). As discussed in §4, numerical integration methods (e.g. Runge-Kutta method) need a shooting approach (in this case the $L$ variable is unknown) to solve eq.s (23), (4) and (5), but each attempt is computationally heavy because it needs the whole solution of the problem.

According to the proposed approach, all kinematic variables are given if the correct value of $\psi_L$ is known.

We can furtherly proceed to the derivation of the static variables. From eq. (44), using the notation (49), the bending moment is obtained:

$$M(u) = EI\,\frac{d\psi}{ds} = x_L\,u\left(qL\,f_{2,3}(u) - F\right) \tag{69}$$

For $M > 0$ substituting eq.s (50) and (54) in (69):

$$M(u) = M\,u\,\frac{f_{2,3}(u)(1+f^*) - f_{2,3}(1)f^*}{f_{2,3}(1)} \tag{70}$$

While for $M = 0$, substituting eq.s (50) and (56) in (69):

$$M(u) = \sqrt{FEI}\,u\left(f_{2,3}(u) - f_{2,3}(1)\right)\sqrt{\frac{2\,\sin\psi_L}{f_{2,3}(1)\left(1 - f_{6,6}(1)\right)}} \tag{71}$$

It is interesting to highlight that the point where the bending moment reaches its maximum does not coincides with the ending points but may lay internally. Differentiating and setting to zero eq. (69), the point where the bending moment reaches its maximum is obtained:

$$u_{Mmax} = \left(\frac{b}{2c}\right)\left[-1 \pm \sqrt{1 + \frac{4c}{b^2}\left(1 - \frac{F}{qL}\right)}\right] \tag{72}$$

The dimensionless form is given, for $M > 0$, using the eq.s (50) and (54) in (72):

$$u_{Mmax} = \left(\frac{b}{2c}\right)\left[-1 \pm \sqrt{1 + \frac{4c}{b^2}\left(\frac{1 + f^*\left(1 - f_{2,3}(1)\right)}{1 + f^*}\right)}\right] \tag{73}$$

While for $M = 0$, using the eq.s (50) and (56) in (72):

$$u_{Mmax} = \left(\frac{b}{2c}\right)\left[-1 \pm \sqrt{1 + \frac{4c}{b^2}\left(1 - f_{2,3}(1)\right)}\right] \tag{74}$$

The physical solutions of (73) and (74) needs positive values. The value of the maximum bending moment is:

$$M_{max} = M(u)\Big|_{u=u_{Mmax}} \tag{75}$$

While the point where the bending moment reaches its maximum has curvilinear abscissa coordinate:

$$s_{Mmax} = s(u)\Big|_{u=u_{Mmax}} \tag{76}$$

And Cartesian coordinates, for $M > 0$

$$x_{Mmax} = u_{Mmax}\,\frac{M}{F}\,f^* \tag{77}$$

$$y_{Mmax} = y(u)\Big|_{u=u_{Mmax}} \tag{78}$$

And for $M = 0$:

$$x_{Mmax} = u_{Mmax}\sqrt{\frac{EI}{F}}\sqrt{\frac{2\,f_{2,3}(1)\sin\psi_L}{1 - f_{6,6}(1)}} \tag{79}$$

$$y_{Mmax} = y(u)\Big|_{u=u_{Mmax}} \tag{80}$$

Using

$$T(s) = -\frac{dM(s)}{ds} \tag{81}$$

and the eq. (23), the shear force is obtained:

$$T(u) = \left(qL\, f_{1,1}(u) - F\right)\cos\psi \tag{82}$$

Using (50) and (54) in (82) one has the dimensionless shear force for $M > 0$:

$$T(u) = F\left[\frac{f_{1,1}(u) + f^*\left(f_{1,1}(u) - f_{2,3}(1)\right)}{f^*\, f_{2,3}(1)}\right]\cos\psi \tag{83}$$

while using (50) and (56), for $M = 0$:

$$T(u) = F\left(\frac{f_{1,1}(u) - f_{2,3}(1)}{f_{2,3}(1)}\right)\cos\psi \tag{84}$$

From previous equations, one also obtains the constrain-reaction force. If $M > 0$, by (83):

$$R = T(u)\Big|_{s=0} = F\left[\frac{1 + f^*\left(1 - f_{2,3}(1)\right)}{f^*\, f_{2,3}(1)}\right] \tag{85}$$

While for $M = 0$ by (84):

$$R = T(u)\Big|_{s=0} = F\left(\frac{1 - f_{2,3}(1)}{f_{2,3}(1)}\right) \tag{86}$$

This one-dimensional model is based on the displacement of the beam centre line; the contact is idealized at the axis level and is represented by a resulting load applied to a specific point. Therefore, the constrain-reaction force $R$ represents the sum of the contact-pressure distribution of a proper three-dimensional contact (Keer and Silva 1972).

Note that in the case $M = 0$ there is a relationship between the constrain-reaction force $R$ and the curvilinear abscissa where the bending moment is maximum $s_{Mmax}$. In $s = s_{Mmax}$ the shear force is equal to zero, so that:

$$R = q\, s_{Mmax} \tag{87}$$

and

$$s_{Mmax} = \frac{F}{q}\left(\frac{1 - f_{2,3}(1)}{f_{2,3}(1)}\right) \tag{88}$$

The mapping introduced in (31) is reversible. This implies that all the equations written so far, can be written according to the curvilinear abscissa $s$. Solving eq. (36) by respect to the dimensionless $u$ variable:

$$u(s) = \left(\frac{b}{2c}\right)\left[-1 \pm \sqrt{1 + \frac{4c}{b^2}\ \frac{s}{L}}\right] \tag{89}$$

For $M > 0$, using (50) and (54):

$$u(s) = \left(\frac{b}{2c}\right)\left[-1 \pm \sqrt{1 + \frac{4c}{b^2}\ \left(\frac{q}{F}\ s\ \frac{f^* f_{2,3}(1)}{1 + f^*}\right)}\right] \tag{90}$$

While, for $M = 0$ by (50) and (56):

$$u(s) = \left(\frac{b}{2c}\right)\left[-1 \pm \sqrt{1 + \frac{4c}{b^2}\ \left(\frac{q}{F}\ s\ f_{2,3}(1)\right)}\right] \tag{91}$$

The physical solutions of (90) and (91) are, again, given by the positive value.

An ordered summary of the equations to facilitate their application, separating $M > 0$ and $M = 0$, is repeated in the Appendix, in dimensionless form.

# 3 Practical use of the solution. Design Charts

One of the advantages of an analytical solution is to present the dimensionless solution through Design Charts.

For the case $M = 0$ , solving the equations (68), setting values for $\psi_L \in \left(0, \frac{\pi}{2}\right)$ one obtains the corresponding values of the dimensionless variable $\frac{F^3}{q^2 EI}$. Being all the variables as only function of the angle $\psi_L$, the solution is therefore known for every combination of $F, q, E, I$. In Fig. 2 the whole solution concerning the kinematic variables is represented, while in Fig. 3 the static variables are given. For the case $M > 0$ the procedure is similar to the previous one. The only difference is that in the equation (67) two dimensionless parameters does occur. Therefore, a simple way is to present graphs as function of $\frac{F^2}{M\,q}$, parameterized with $\frac{FEI}{M^2}$. In Fig. 4, 5, 6, and 7 the graphs of the kinematic variables are shown, while Fig. 8, 9, 10, 11 and 12 regard the static variables. One can use these graphs for given loads as well as for given displacements and/or rotation. To get all these graphs, it is not necessary to carry on attempts for $\psi_L$, since they are derived spanning its values between 0 to $\frac{\pi}{2}$; therefore, the computational task is direct. To facilitate the practical use of the graphs and to obtain a wide range of solutions the abscissa is presented in logarithmic scale.

# 4 Numerical and experimental validations

## 4.1 Comparison between Analytical, Runge-Kutta and F.E.M.

In this sub-paragraph a numerical application is shown. The goal is to validate the analytical solutions exposed in §2 when both ending load and bending moment are present. Comparison is carried on with the numerical solutions obtained by Runge-Kutta method and F.E.A. The results obtained using a simpler linear curvilinear abscissa map is also given to highlight the solution progress when parabolic mapping is adopted.

To resolve eq. (67) (in the same way for eq. (68)), knowing the load conditions and the geometric and elastic data of the beam shown in the Fig. 13 (i.e. known the dimensionless parameters $\frac{F^2}{Mq}$ and $\frac{FEI}{M^2}$), an attempt method is required. For this case the bisection method is used with a

permissible error of $10^{-12}$ of the ending angle $\psi_L$ and the result is reached with 7 iterations. Generally, with this tolerance and an initial search interval of bisection method as $[\psi_a, \psi_b] = \left[\varepsilon, \frac{\pi}{2} - \varepsilon\right]$ with $\varepsilon = 0.017\ rad \cong 1\ deg$, the number of iterations is limited on 10. With the R-K numerical method the equations to solve are (4), (5) and (23) with the initial condition (27), (29) and the boundary value problem (26). It is essential to notice that it is not possible to directly apply the R-K integration method, inasmuch the variable $L$ (inflection length) is unknown; this implies that the procedure needs to be supported by an attempt (shooting) method too. In this case, the bisection method is still used to get the unknown variable $L$, applying a tolerance of $10^{-5}$ $m$ on equation (26); convergence is reached after 18 iterations. In the finite element method $10^3$ beam elements are used (two nodes) and gap-elements are employed to account of soil contact. The analytical linear map $s(x) = \frac{L}{x_L}\, x$ is easy to get from the equations shown in §2 and in the appendix, imposing $m(\psi_L) = n$ i.e. $b(\psi_L) = 1$ and $c(\psi_L) = 0$. The graphical results are shown in Fig. 13. For sake of clarity in Table 1 the values of the $y_L$ displacement component of the lifting point and the relative errors between the methods are given, together with the $\psi_L$ angle results. The values of the analytical method with parabolic curvilinear abscissa map, R-K integration method and the F.E.M. are matching well. Otherwise, the results of the analytical method with linear mapping differs significantly from all others; therefore, its use is not recommended when large displacements and rotations occur. In Fig. 14 the graph of $s(x)$ is shown, comparing all the methods mentioned above and confirming again the adherence of the numerical results with the analytical method when the curvilinear abscissa is mapped through a parabola. The location of the internal point of the interpolating parabola is chosen according to eq. (35); other intermediate locations have been explored, but the accuracy keeps similar when moving the internal point along the inflected part of the beam. Therefore, the (35) can be considered as a useful choice.

## 4.2 Experimental validations

A number of experimental tests have been performed to check the reliability of the proposed analytical method and the numerical results used for comparison. Experimental analysis are here conducted avoiding end bending moment, for a simpler realization of the experimental setting.

The tests were performed with a rectangular section steel beam having wide $d = 19.95 \cdot 10^{-3}\, m$, thick $h = 2.95 \cdot 10^{-3}\, m$ and Young's modulus $E = 209\, GPa$. The total length of the beam is $L_{tot} = 2.670$ m and its density is $\rho = 7763\ \frac{kg}{m^3}$; therefore the distributed load for unit length due to own weight is $q_w = 4.48\ \frac{N}{m}$. The tests are performed with displacement control imposing appropriate loads at the free-end of the beam (Fig.15). The loading wire is connected to a load cell to measure the actual force. The contact point (Fig.16) is determined by measuring the length of the segment $L_{tot} - L$ that keeps in contact with the floor. Its evaluation is obtained by dragging a thin layer (thick $10^{-4}\, m$) withheld by two magnetic rings, to guarantee repetitive values for the drag and resistance force for all tests. To evaluate the behaviour of the system and the reliability of the analytical and numerical methods, if the distributed weight load varies, additional independent weights are piled on the beam. Each single added piece has a mass of $5 \cdot 10^{-3}\, kg$, while the dimensions and assembly distance are shown in Fig.17. Three tests were performed for given displacements (200, 400, 600 mm) and this procedure was repeated when additional weight are piled on the beam (zero up to four tiers), so that curvature increases accordingly.

Indeed, the added masses are not located in the centre of the beam section but they accumulate over the section top. We studied how this geometric shift affects the results by FEM and we deduced that it contributes less than a 0.02 % of the end displacement. Considering the testing scenario, it remains within the range of experimental repeatability.

In the Tables 2, 3, 4, 5 and 6 the average values of force, distance of contact point and lifting point angle of the three tests are reported. The values of the lifting point angles are extracted from image analyses. In the results reported in the tables, for the calculation of the contact distance a contact threshold of $10^{-4}\, m$ is considered, namely any point having a vertical distance

from the contact layer $\leq 10^{-4}\, m$ is in contact. In this case, the contact-threshold value is set equal to the thickness of the layer used in the tests, to gain a real comparison between the tests and the analytical data and the numerical computations. The application of a threshold is particularly useful since the contact point is reached almost asymptotically; therefore, its determination becomes non-reliable if a smaller value of the threshold is taken into account.

The results of the experimental tests show a high adherence with the proposed analytical model and with the numerical comparison methods. The agreement is not affected by the increase of the applied loads (added weights), that implies a considerable growth of the slope of the inflected beam.

Resuming all test results, both cases of the presence or not of end-bending moment have been explored. All the numerical or experimental validations involves very high displacements and ending angles. From the examples reported we can state that the proposed analytical procedure is reliable for a wide range of cases, comprising small, moderate up to large deformations.

## Conclusion

Analytical curvilinear abscissa mapping method is discussed in this paper to solve the problem of the Heavy Elastica with soil interaction when loaded by force and bending moment at the free-end. The adopted hypotheses regard the linear relationship of stress and strain, isotropy and homogeneity of the material and the preservation of the section moment of inertia. Axial elongation and shear-strain energy contributions have been neglected. The considered loading conditions are such that inflection points (points of zero curvature) dos not occur. The only mathematical hypothesis is that the curvilinear abscissa can be expressed through a second-degree polynomial with respect to the Cartesian abscissa. The coefficients of the polynomial are determined by imposing three points of the interpolating parabola. This requires the introduction of a closing equation which depends on one kinematic-variable of the problem ($\psi_L$). Introducing this hypothesis in the system of equations, the solution of the Heavy Elastica problem is reached in an

analytical form. The obtained analytical solution has the same complexity of the classical Elastica, subjected to end-concentrated forces and moment only. The analytical solution has a computational advantage (less computational time) with respect to numerical integration methods. In fact, both need an attempt (shooting) method (as the classical Elastica), but the analytical method avoids the lengthy integration over the full dimension of the beam for each attempt. Moreover, the analytical solution admits a dimensionless form, which is shown in the Design Charts of §3, representing the solutions in the whole field of applications i.e. for each combination of $F, q, M, E, I$ or any imposed displacement and/or rotation. A comparison between the proposed analytical solution (parabolic curvilinear abscissa mapping), Runge-Kutta integration method and finite element method is reported in § 4.1, where the convergence of the three approaches and therefore the validity of the method is shown. The computation of the $s(x)$ for the Runge-Kutta and F.E. results showed a very good agreement with the assumption of a parabolic trend for $s(x)$. We also showed that a simpler (linear) mapping implies a significant reduction of the accuracy; its use is not recommended for large displacements and rotations. Some experimental tests are reported in § 4.2. The analytical solution with parabolic curvilinear abscissa mapping agrees with the experimental results validating the proposed model, even if the deformations are increased by adding mass to the beam. Experimental evidences also show that the first contact point varies in great accordance with the analytical previsions. The precision measuring of this point is essential since it indicates the inflection length of the beam.

The experimental measurement of the first contact point implies the use of a layer of finite thickness, which must be taken into account as contact threshold for numerical and analytical comparisons.

## Acknowledgments

The authors wish to acknowledge PhD Emanuele Marotta for the contribution given in the experimental validation.

# Appendix

The aim of this paragraph is to concisely summarize the equations obtained previously. The cases $M > 0$ and $M = 0$ are divided, providing a chronological (not mandatory for application) order of formula applications, useful for the implementation of the model. The equations used for both cases are:

$$u = \frac{x}{x_L} \quad \in [0,1] \tag{A.1}$$

$$b(\psi_L) = \frac{m^2 - n}{m\,(m-1)} \tag{A.2}$$

$$c(\psi_L) = \frac{n - m}{m\,(m-1)} \tag{A.3}$$

$$n = \frac{1}{2} \tag{A.4}$$

$$m(\psi_L) = \frac{n}{cos\left(\frac{\psi_L}{2}\right)} \tag{A.5}$$

The only condition to keep in mind is that the first equation to be calculated is the one allowing the calculation of $\psi_L$ variable, i.e. the eq. (78) for $M > 0$ and (79) for $M = 0$ .

The following compact notation is used:

$$f_{a_1,a_2}(t) = 1 - \frac{b}{a_1}\,t - \frac{c}{a_2}\,t^2 \quad with\ a_1, a_2 \in \mathbb{R}$$

The formulas for the two distinct cases are summarized.

**Case $M > 0$ :**

$$f^*\left(\psi_L, \frac{FEI}{M^2}\right) = \frac{1}{2}\left(\frac{f_{3.6}(1)}{1 - f_{6,6}(1)}\right)\left[-1 \pm \sqrt{1 + 8\left(\frac{FEI}{M^2}\right)\left(\frac{f_{2,3}(1)\left(1 - f_{6,6}(1)\right)}{\left(f_{3,6}(1)\right)^2}\right)}\right] \tag{A.6}$$

$$\sin\psi\ \left(\psi_L\ , u, \frac{FEI}{M^2}\right) = \sin\psi_L\ u^2\ \frac{(1+f^*)\ f_{3,6}(u) - f^*\ f_{2,3}(1)}{(1+f^*)\ f_{3,6}(1) - f^*\ f_{2,3}(1)} \tag{A.7}$$

$$\frac{F^2}{Mq} = \frac{f_{2,3}(1)\ (f^*)^2}{(1+f^*)} \int_0^1 \frac{du}{\sqrt{1-sin^2\psi}} \tag{A.8}$$

$$\frac{F}{M}\ y(u) = f^* \int_0^u \frac{\sin\psi}{\sqrt{1-sin^2\ \psi}}\ d\tilde{u} \tag{A.9}$$

$$\frac{F}{M}\ x_L\left(\psi_L\ , \frac{FEI}{M^2}\right) = f^* \tag{A.10}$$

$$\frac{q}{F}\ L = \frac{1+f^*}{f^* f_{2,3}(1)} \tag{A.11}$$

$$\frac{q}{F}\ s(u) = \frac{(1+f^*)\big(1-f_{1,1}(u)\big)}{f^* f_{2,3}(1)} \tag{A.12}$$

$$u(s) = \left(\frac{b}{2c}\right)\left[-1 \pm \sqrt{1+\frac{4c}{b^2}\ \left(\frac{q}{F}\ s\ \frac{f^*\ f_{2,3}(1)}{1+f^*}\right)}\right] \tag{A.13}$$

$$u_{Mmax} = \left(\frac{b}{2c}\right)\left[-1 \pm \sqrt{1+\frac{4c}{b^2}\ \left(\frac{1+f^*\ \left(1-f_{2,3}(1)\right)}{1+\ f^*}\right)}\right] \tag{A.14}$$

$$\frac{q}{F} s_{Mmax} = \frac{q}{F} s(u)\Big|_{u=u_{Mmax}} \tag{A.16}$$

$$\frac{F}{M} x_{Mmax} = u_{Mmax}\ f^* \tag{A.17}$$

$$\frac{F}{M} y_{Mmax} = \frac{F}{F} y(u)\Big|_{u=u_{Mmax}} \tag{A.18}$$

$$\frac{M(u)}{M} = u\ \frac{f_{2,3}(u)(1+f^*) - f_{2,3}(1)f^*}{f_{2,3}(1)} \tag{A. 19}$$

$$\frac{M_{max}}{M} = \frac{M(u)}{M}\Big|_{u=u_{Mmax}} \tag{A. 20}$$

$$\frac{T(u)}{F} = \frac{f_{1,1}(u) + f^*\left(f_{1,1}(u) - f_{2,3}(1)\right)}{f^*\, f_{2,3}(1)}\ \cos\psi \tag{A. 21}$$

$$\frac{R}{F} = \frac{1 + f^*\left(1 - f_{2,3}(1)\right)}{f^*\, f_{2,3}(1)} \tag{A. 22}$$

Case $\boldsymbol{M = 0}$ :

$$\sin\psi\ (\psi_L\ , u) = \sin\psi_L\ u^2\ \frac{f_{3,6}(u) - f_{2,3}(1)}{1 - f_{6,6}(1)} \tag{A. 23}$$

$$\frac{F^3}{q^2 EI} = \frac{2\left(f_{2,3}(1)\right)^3 sin\ \psi_L}{1 - f_{6,6}(1)} \left(\int_0^1 \frac{du}{\sqrt{1 - sin^2\psi}}\right)^2 \tag{A. 24}$$

$$\frac{F}{M}\ y(u) = \sqrt{\frac{2\ f_{2,3}(1)\sin\psi_L}{1 - f_{6,6}(1)}}\ \int_0^u \frac{\sin\psi}{\sqrt{1 - sin^2\psi}}\ d\tilde{u} \tag{A. 25}$$

$$\sqrt{\frac{F}{EI}}\ x_L(\psi_L) = \sqrt{\frac{2\ f_{2,3}(1)\sin\psi_L}{1 - f_{6,6}(1)}} \tag{A. 26}$$

$$\frac{q}{F}\ L = \frac{1}{f_{2,3}(1)} \tag{A. 27}$$

$$\frac{q}{F}\ s(u) = \frac{1 - f_{1,1}(u)}{f_{2,3}(1)} \tag{A. 28}$$

$$u(s) = \left(\frac{b}{2c}\right)\left[-1 \pm \sqrt{1 + \frac{4c}{b^2}\ \left(\frac{q}{F}\ s\ f_{2,3}(1)\right)}\right] \tag{A. 29}$$

$$u_{Mmax} = \left(\frac{b}{2c}\right)\left[-1 \pm \sqrt{1 + \frac{4c}{b^2}\ \left(1 - f_{2,3}(1)\right)}\right] \tag{A. 30}$$

$$\frac{q}{F} s_{Mmax} = \frac{q}{F} s(u)\Big|_{u=u_{Mmax}} \tag{A. 31}$$

$$\sqrt{\frac{F}{EI}}\ x_{Mmax} = u_{Mmax}\sqrt{\frac{2\, f_{2,3}(1)\sin\psi_L}{1 - f_{6,6}(1)}} \tag{A. 32}$$

$$\sqrt{\frac{F}{EI}} y_{Mmax} = \sqrt{\frac{F}{EI}} y(u)\Big|_{u=u_{Mmax}} \tag{A. 33}$$

$$\frac{M(u)}{\sqrt{FEI}}\, u\left(f_{2,3}(u) - f_{2,3}(1)\right)\sqrt{\frac{2\ \sin\psi_L}{f_{2,3}(1)\left(1 - f_{6,6}(1)\right)}} \tag{A. 34}$$

$$\frac{M_{max}}{\sqrt{FEI}} = \frac{M(u)}{\sqrt{FEI}}\Big|_{u=u_{Mmax}} \tag{A. 35}$$

$$\frac{T(u)}{F} = \left(\frac{f_{1,1}(u) - f_{2,3}(1)}{f_{2,3}(1)}\right)\cos\psi \tag{A. 36}$$

$$\frac{R}{F} = \frac{1 - f_{2,3}(1)}{f_{2,3}(1)} \tag{A. 37}$$

# References


Antman S. S. 1995. Nonlinear Problems of Elasticity-[$2^{nd}$ edition]. Springer Verlag. New York.

Barber J.R., 2018. Contact Mechanics. Solid Mechanics and Its Applications. Springer International Publishing.

Chen L. 2010. An integral approach for large deflection cantilever beams. International Journal of Non-Linear Mechanics, 45, 301-305.

DaDeppo D.A. and Schmidt R. 1971. Analysis of Nonlinear Deflections of Fibers. Textile Research Journal, vol. 41, 11, 911-915.

Fertis D. G. 2006. Nonlinear Structural Engineering. Springer-Verlag Berlin Heidelberg.

Feodosyev V.I., 1977. Selected Problems and Questions in Strength of Materials. Translated from the Russian by M. Konyaeva. Mir,Moscow.

Frish-Fay R., 1962. Flexible bars, Butterworths. London.

Ghuku S. and Saha K. N. (2016). A theoretical and experimental study on geometric nonlinearity of initially curved cantilever beams. Engineering Science and Technology, an International Journal, 19, 135-146.

Holden J.T. 1972. On the Deflection of Thin Beams. International Journal of Solids and Structures, vol.8, 1051-1055.

Iandiorio C., Salvini P. 2020. Large displacements of slender beams in plane: Analytical solution by means of a new hypergeometric function. International Journal of Solid and Structures, 185-186, 467-484.

Keer L.M. and Silva M.A.G., 1972. Two mixed problems for a semi-infinite layer. ASME Journal of Applied Mechanics, 39, 1121-1124.

Kim J.H., Ahn Y.J. and Jang Y.H. and Barber J.R. 2014. Contact problems involving beams. International Journal of Solid and Structures, 51, 4435-4439.

Kimiaeifar A., Tolou N., Barari A. and Herder J.L. 2014. Large deflection analysis of cantilever beam under end-point and distributed load. Journal of the Chinese Institute of Engineers, 37, 438-445.

Landau L.D. and Lifšits E.M. 1963. Theory of Elasticity. Theoretical Physics. Pergamon Press, London.

Majidi C. , O'Reilly O. M. and Williams J. A. 2012. On the stability of a rod adhering to a rigid surface: Shear-induced stable adhesion and the instability of peeling. Journal of the Mechanics and Physics of Solids, 60, 827–843.

Maleki M., Tonekaboni S.A.M. and Abbasbandy S. 2014. A homotopy analysis solution to large deformation of beams under static arbitrary distributed load. Applied Mathematical Modelling, 38,355-368.

Mingari Scarpello G and Ritelli Daniele 2011. Exact Solutions of Nonlinear Equation of Rod Deflections Involving the Lauricella Hypergeometric Functions. International Journal of mathematics and Mathematical Sciences.

Obreimoff J.W. 1930. The splitting strength of mica. Proc. Ro. Soc. of London ,v. 125, pp. 290-297.

O'Reilly O. M. 2017. Modeling Nonlinear Problems in the Mechanics of Strings and Rods: The Role of the Balance Laws. Springer Nature, Switzerland.

Popov V. L. 2017. Contact Mechanics and Friction. Springer-Verlag, Berlin.

Reissner, E. 1972. On one-dimensional finite-strain beam theory: The plane problem. Journal of Applied Mathematics and Physics (ZAMP) 23, 795–804.

Rohde F. 1953. Large deflections of a cantilever beam with uniformly distributed load. Quart. Appl. Math. 11, 337–338.

Schmidt R. and DaDeppo D.A. 1970. Large deflections of a heavy cantilever beams and columns. Quartely of Applied Mathematics, 28, 441-444.

Schmidt R. and DaDeppo D.A. 1971. Approximate Analysis of Large Deflections of Beams. ZAMM Journal of Applied Mathematics and Mechanics, 51,233-234.

Solyaev Y., Ustenko A. and E. Lykosova 2019. Approximate Analytical Solution for a Unilateral Contact Problem with Heavy Elastica. Lobachevskii Journal of Mathematics. Vol. 40, 7, 1110-1115.

Wang C.Y. 1981. Large Deformations of a Heavy Cantilever. Quarterly of Applied Mathematics, 39, 261-273.

Wang C.Y. 1986. A Critical Review of the Heavy Elastica. International Journal of Mechanical Sciences, vol. 28, 8, 549-559.

Wang T.M., Lee S.L. and Zienkiewicz O.C. 1961. A Numerical Analysis of Large Deflection of Beams. International Hournal of Mechanical Sciences, vol.3, 210-228.

Wnuk M.P., 1990. Nonlinear Fracture Mechanics. CISM International Centre for Mechanical Sciences. Springer-Verlag, Wien.

Yi Xiao 2001. Large Deflection of Catnilever Beam with Uniformly Distributed Load Using Homotopy Analisys Method. Advanced Materials Research, vol. 250, 1222-1225.

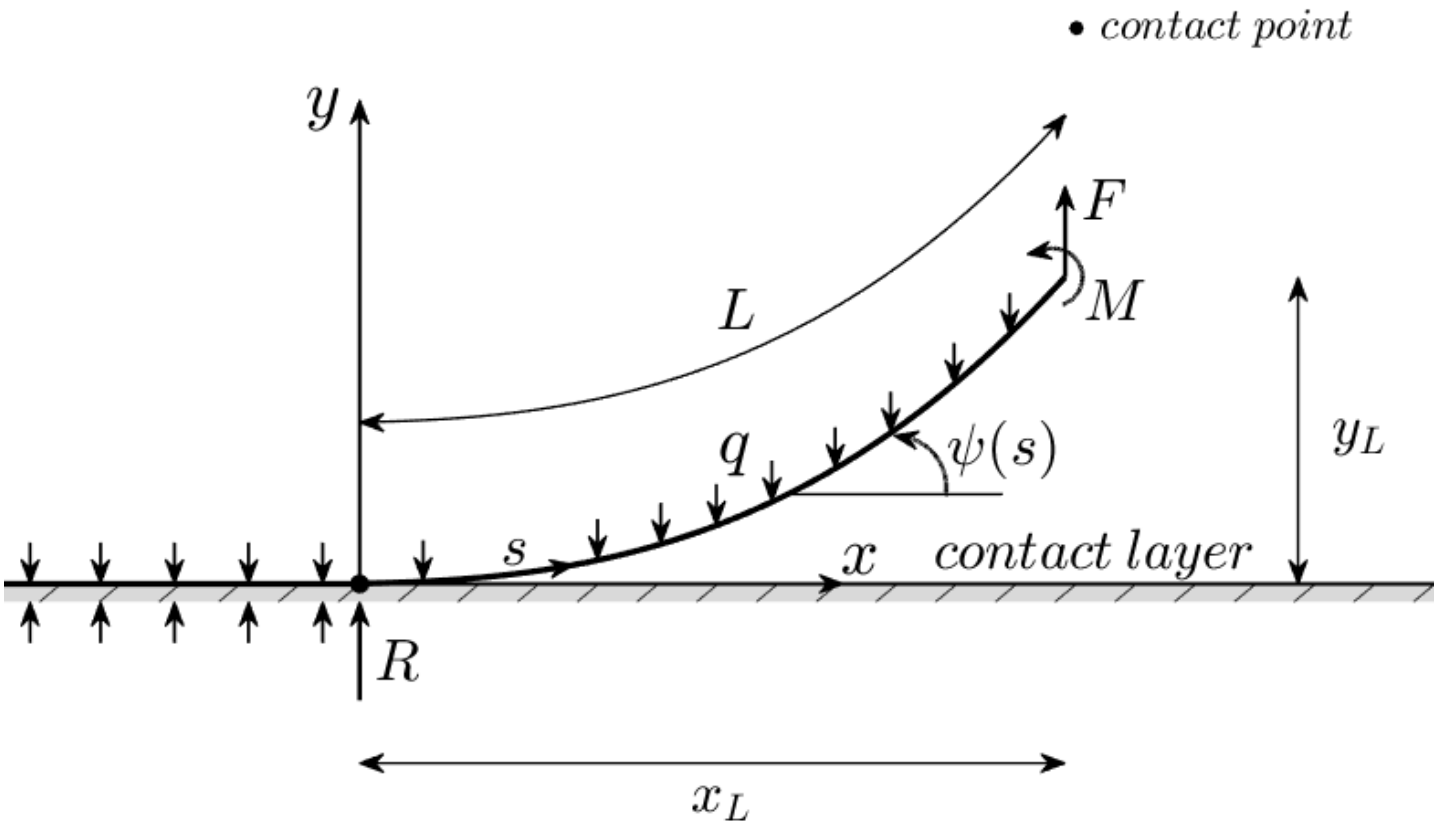


**Fig.1** Deformed configuration scheme

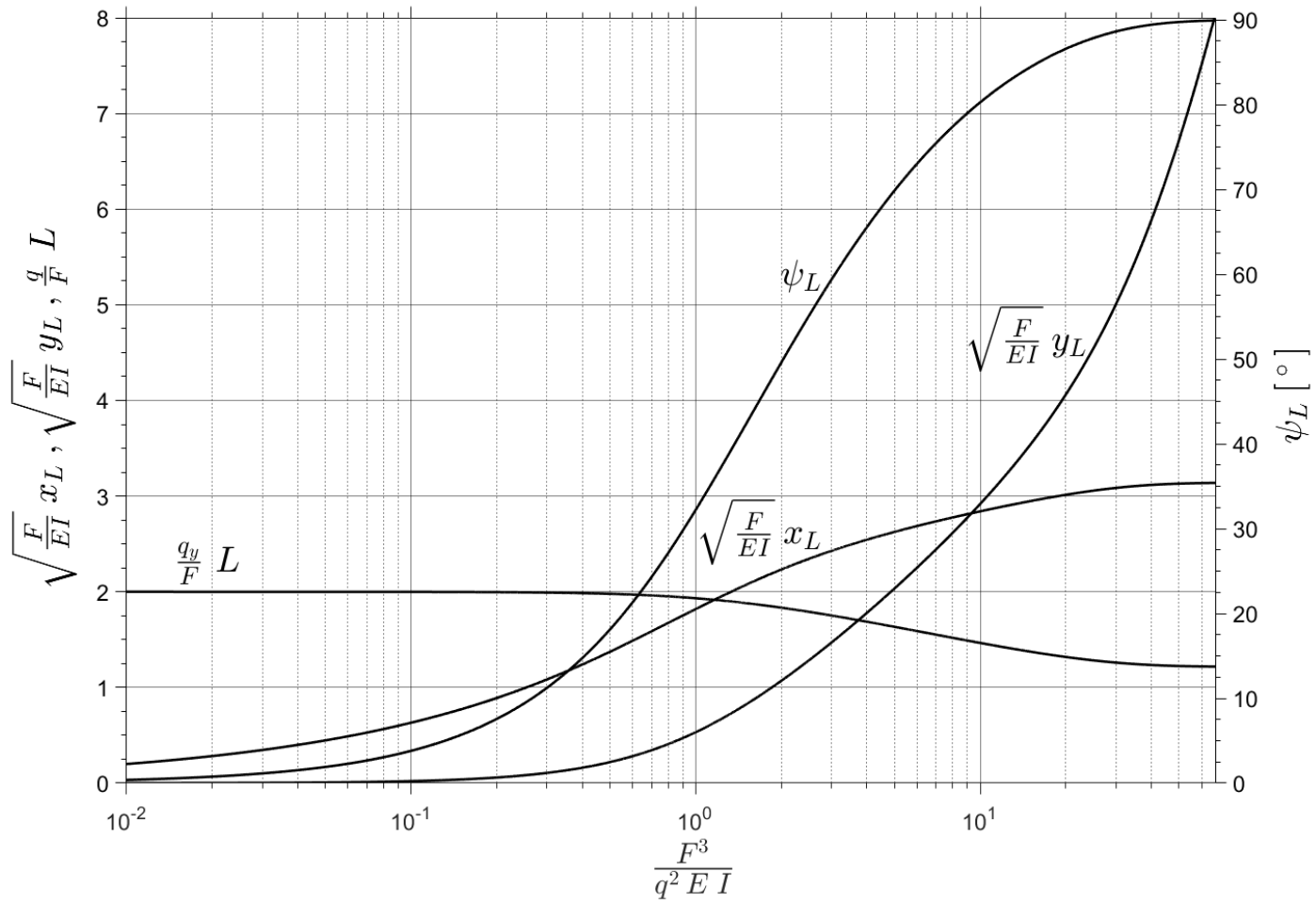


**Fig.2** Kinematic variable values - case $M = 0$

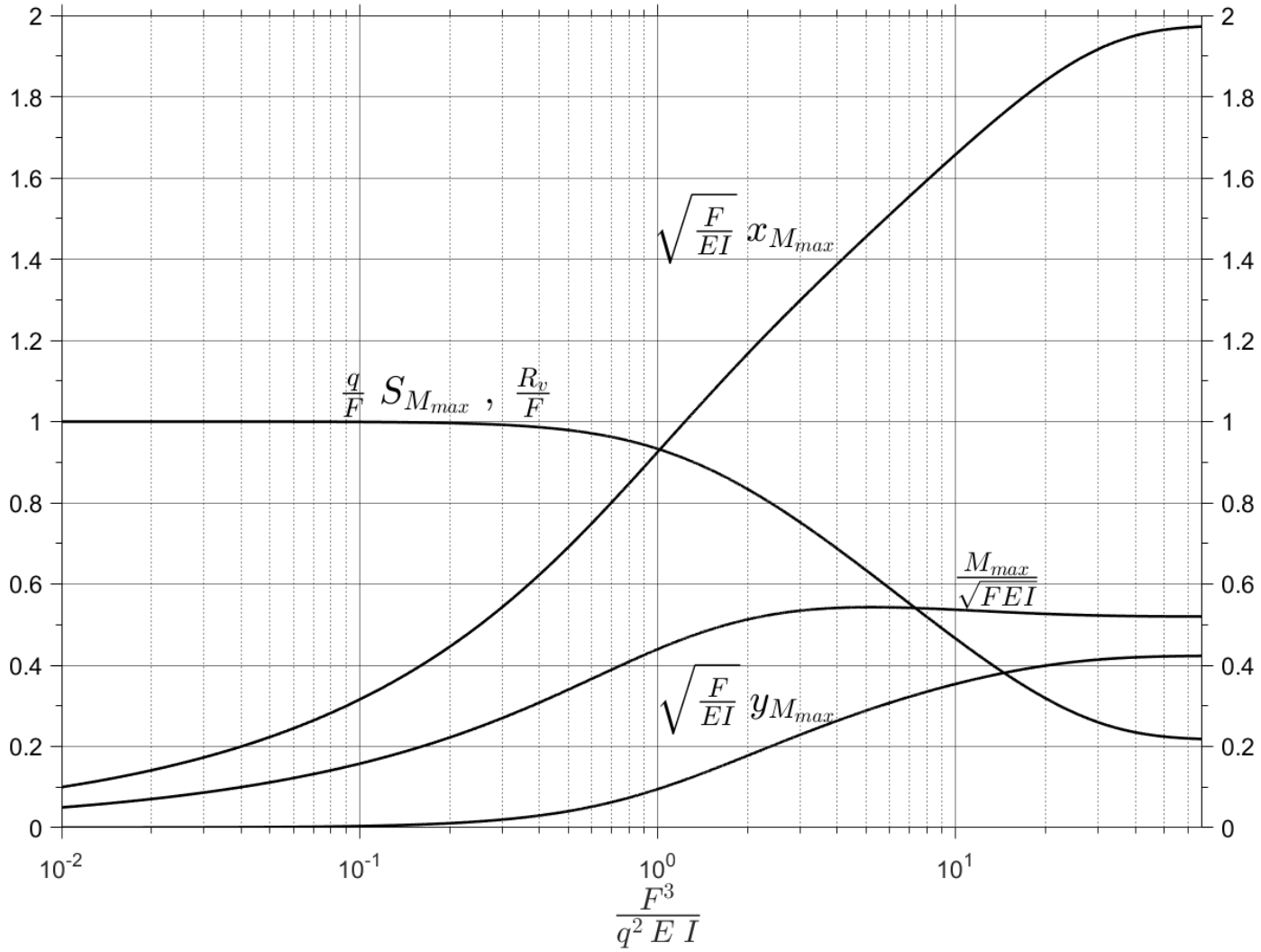


**Fig.3** Static variable values - case $M = 0$

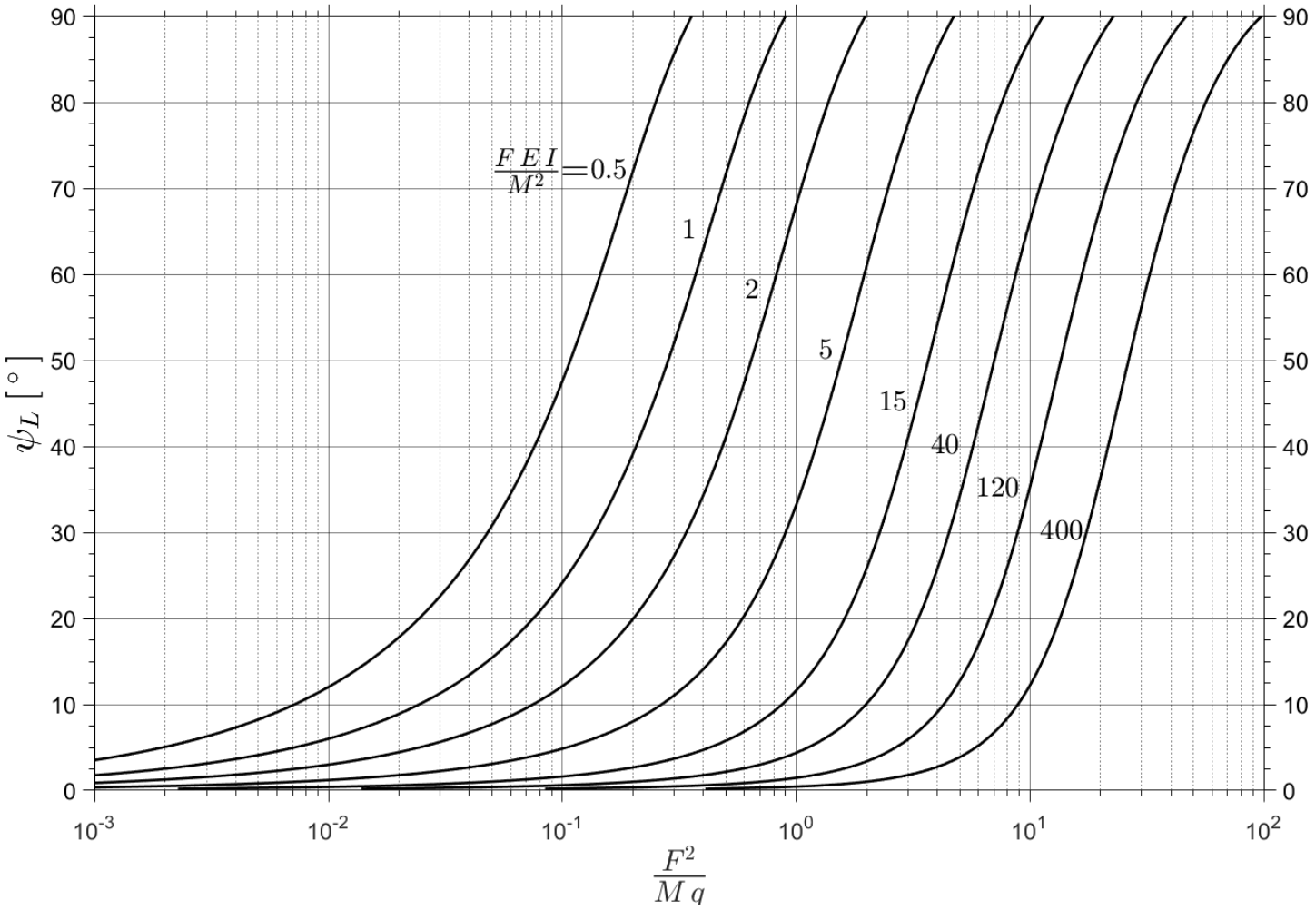


**Fig.4** Ending angle $\psi_L$ - case $M > 0$

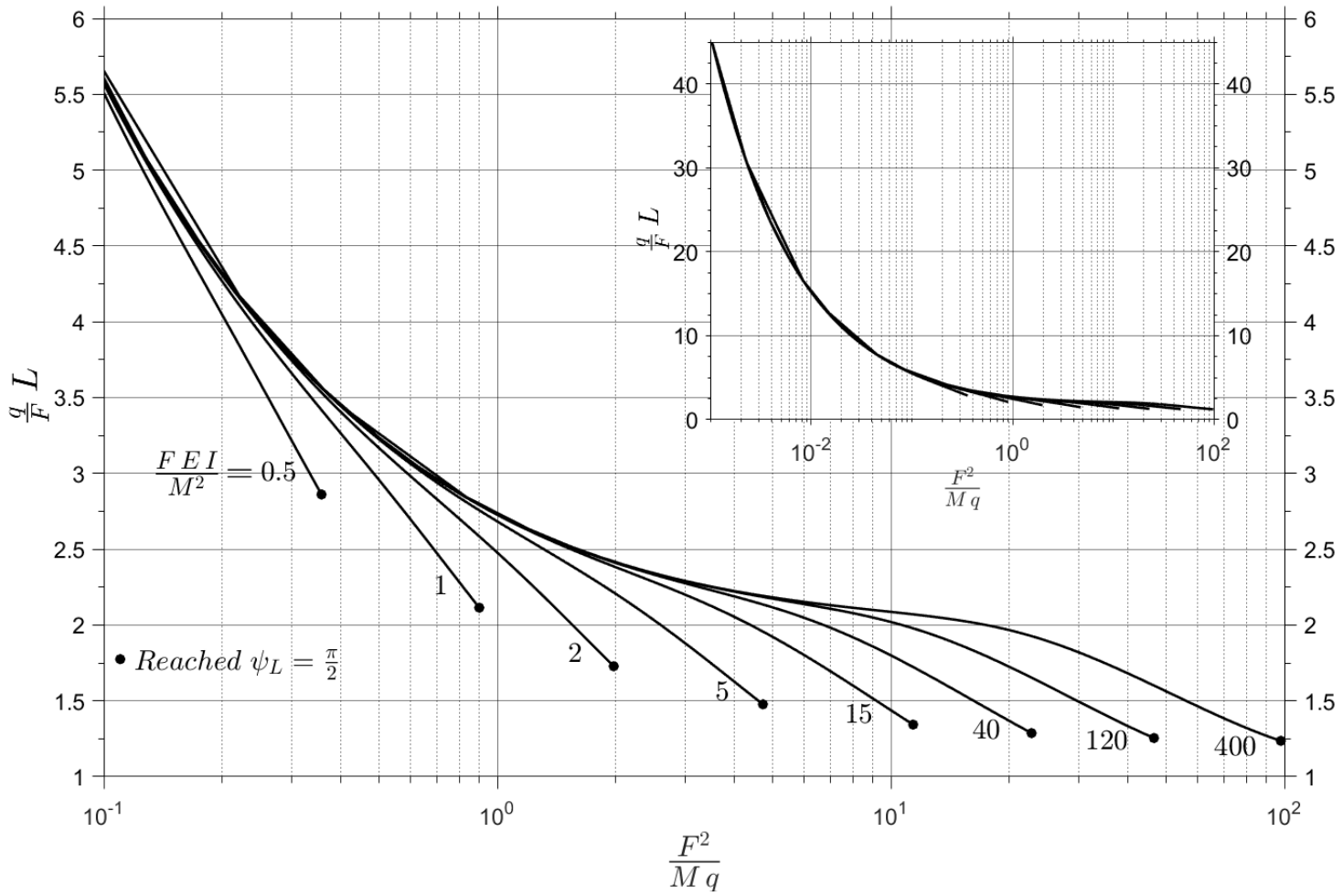


**Fig.5** Dimensionless inflected length - case $M > 0$

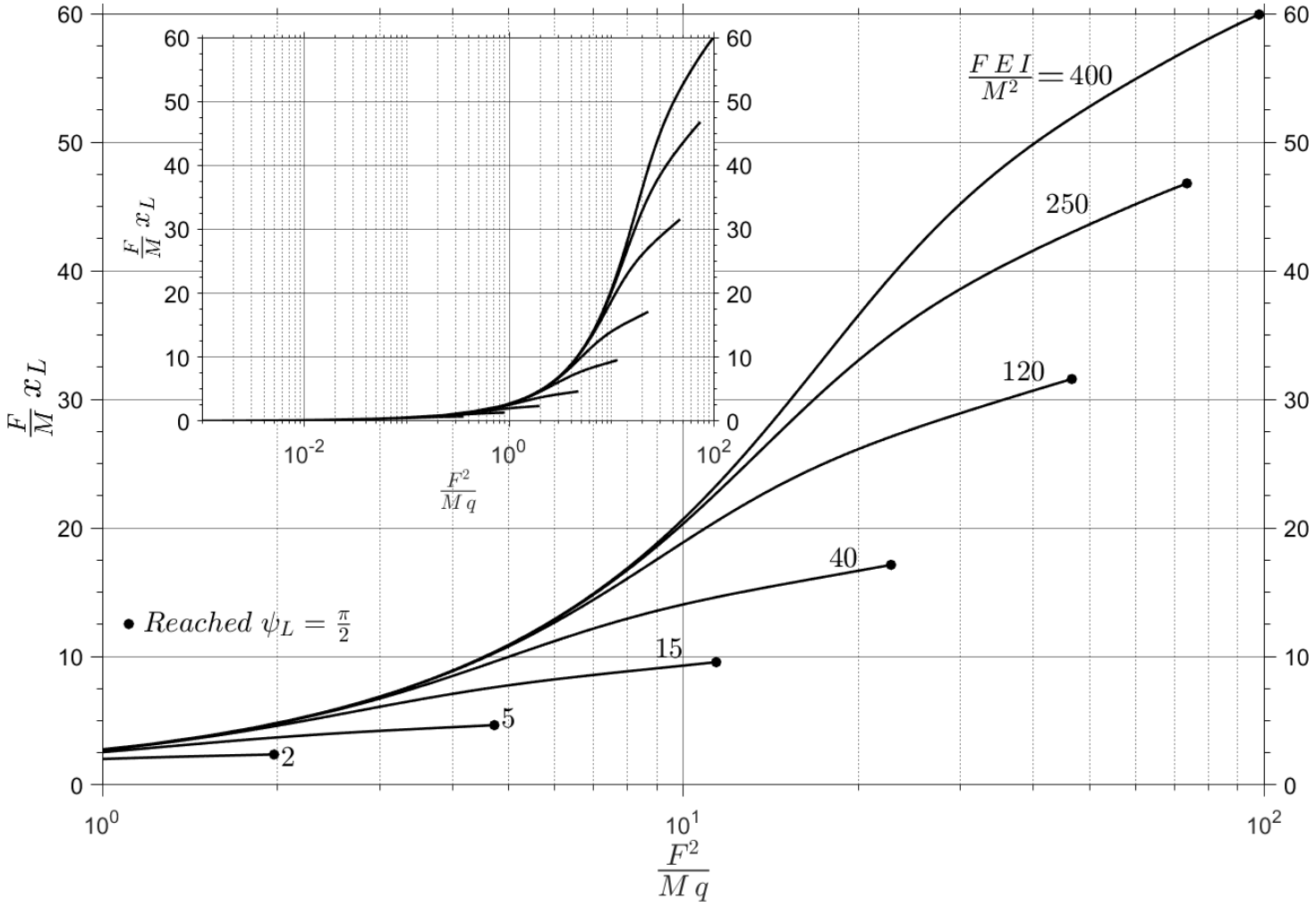


**Fig.6** Dimensionless abscissa of the lifting point - case $M > 0$

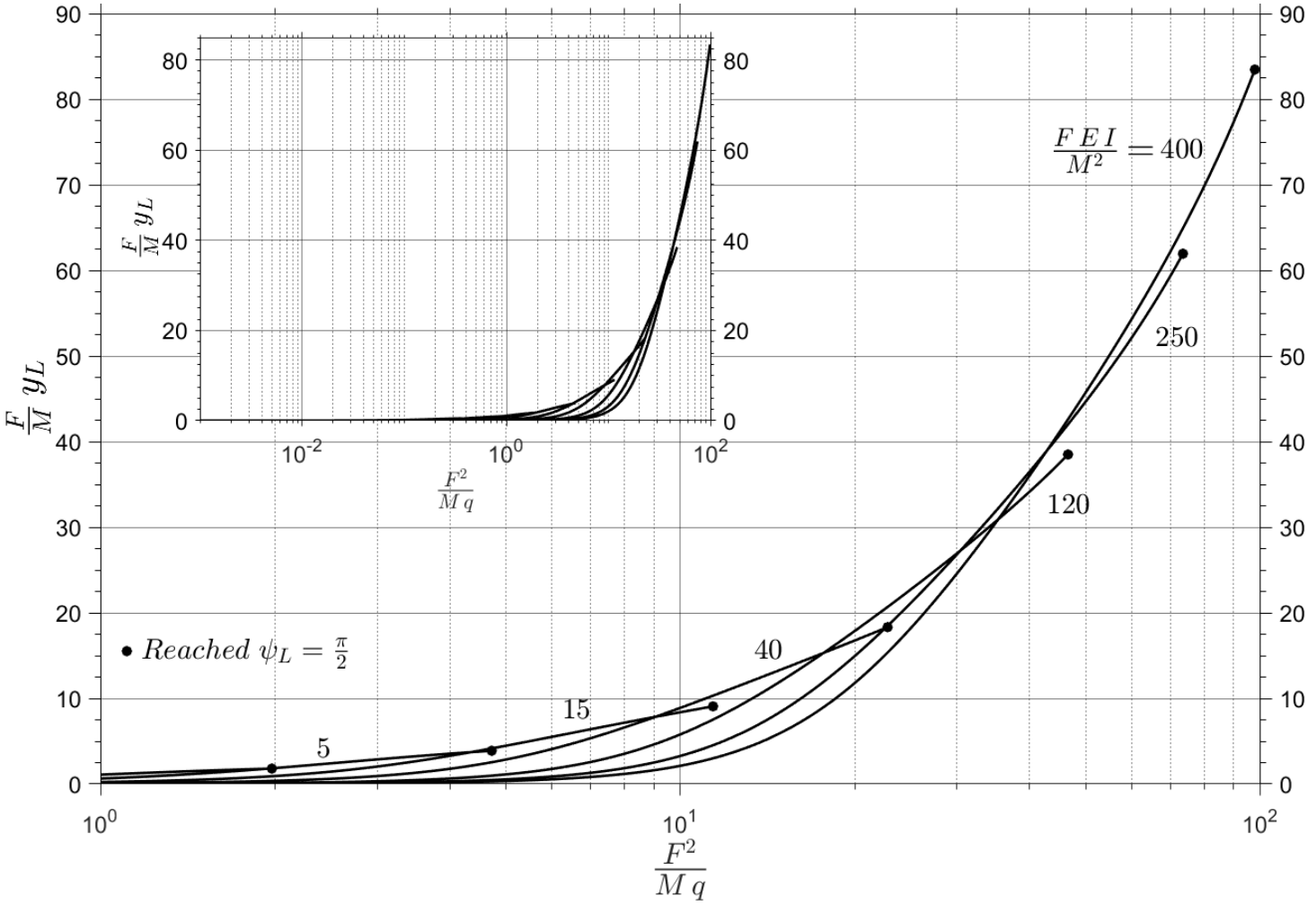


**Fig.7** Dimensionless ordinate of the lifting point - case $M > 0$

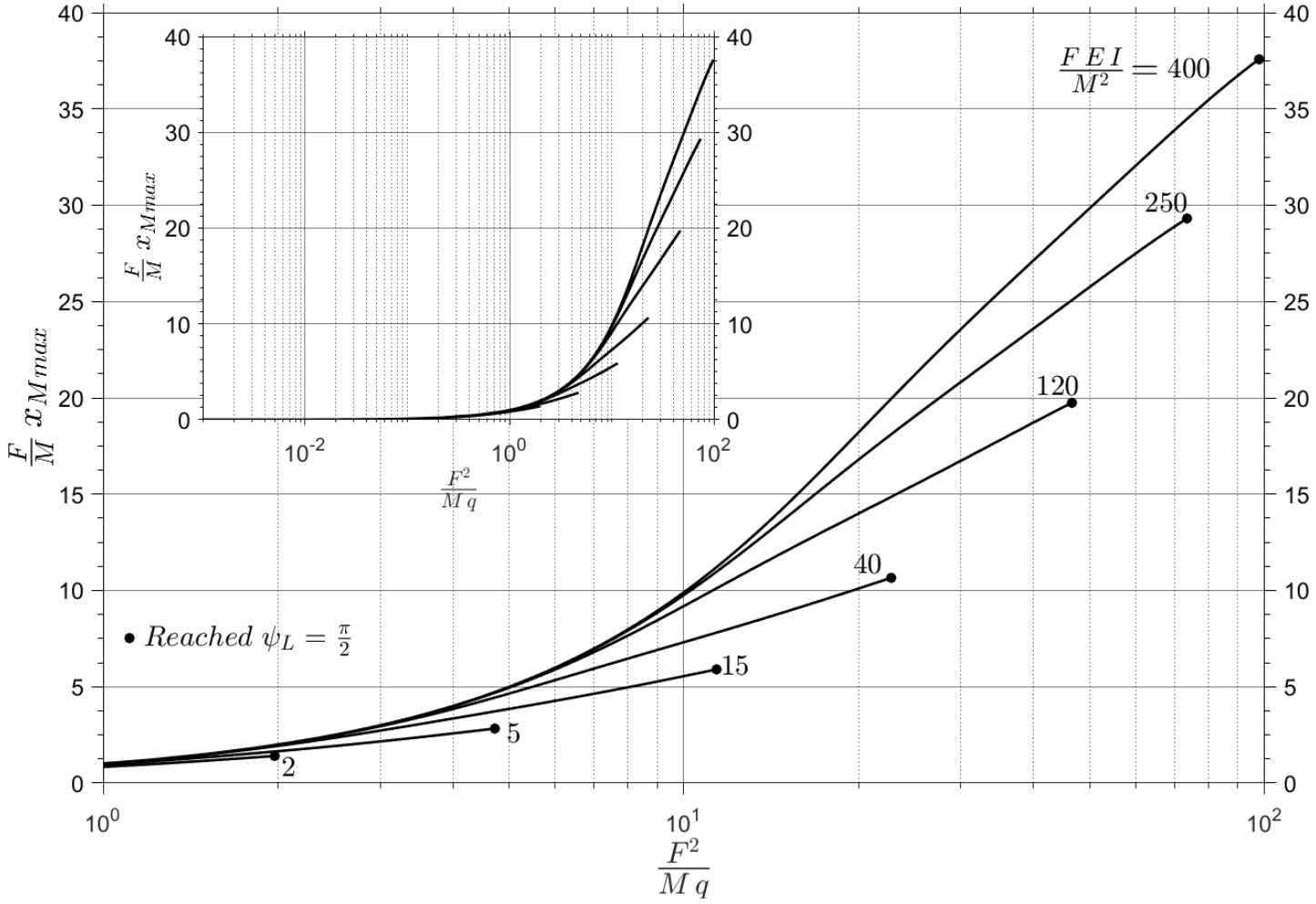


**Fig.8** Dimensionless abscissa where bending moment reaches its maximum value - case $M > 0$

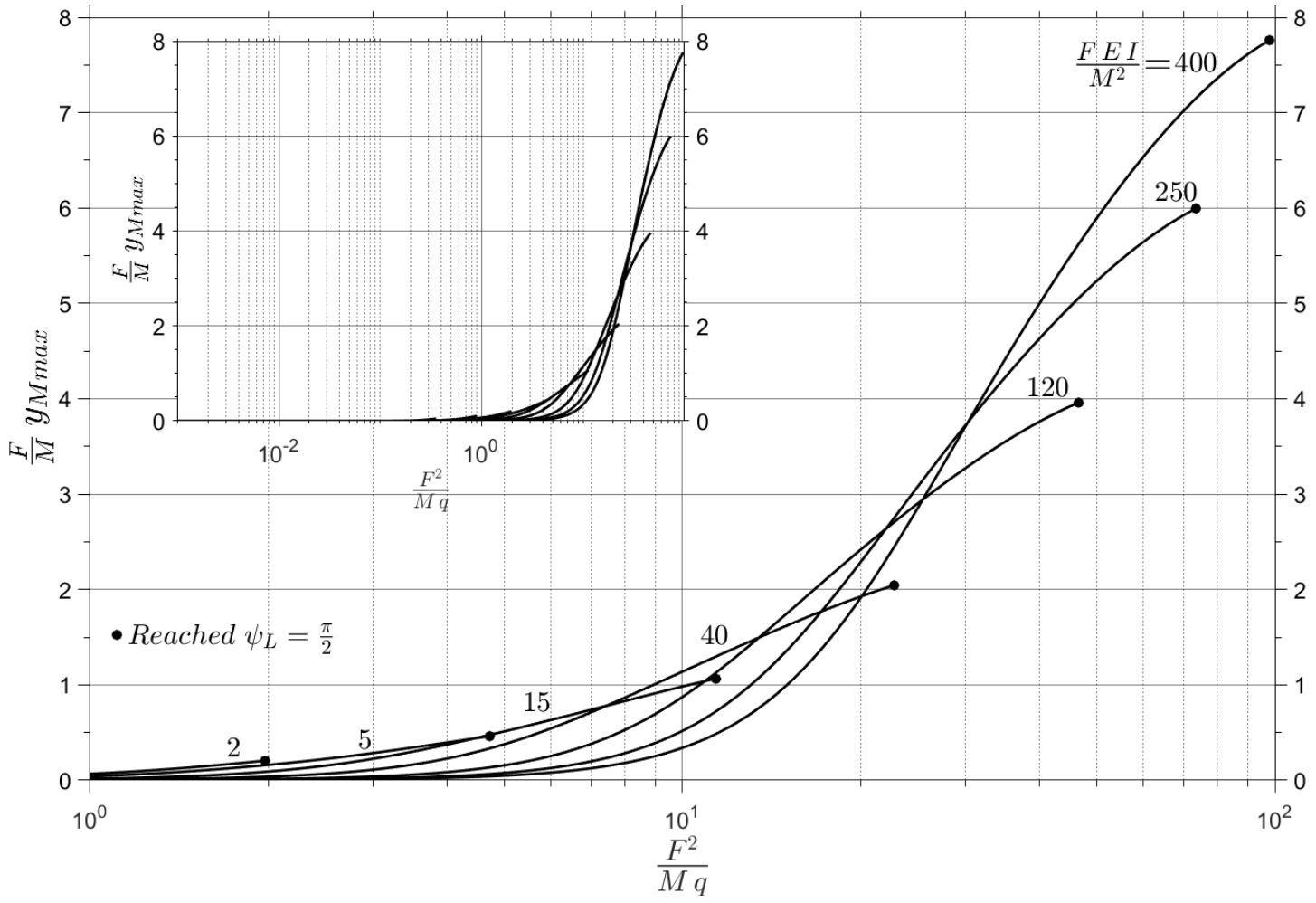


Fig.9 Dimensionless ordinate where bending moment reaches its maximum value - case $M > 0$

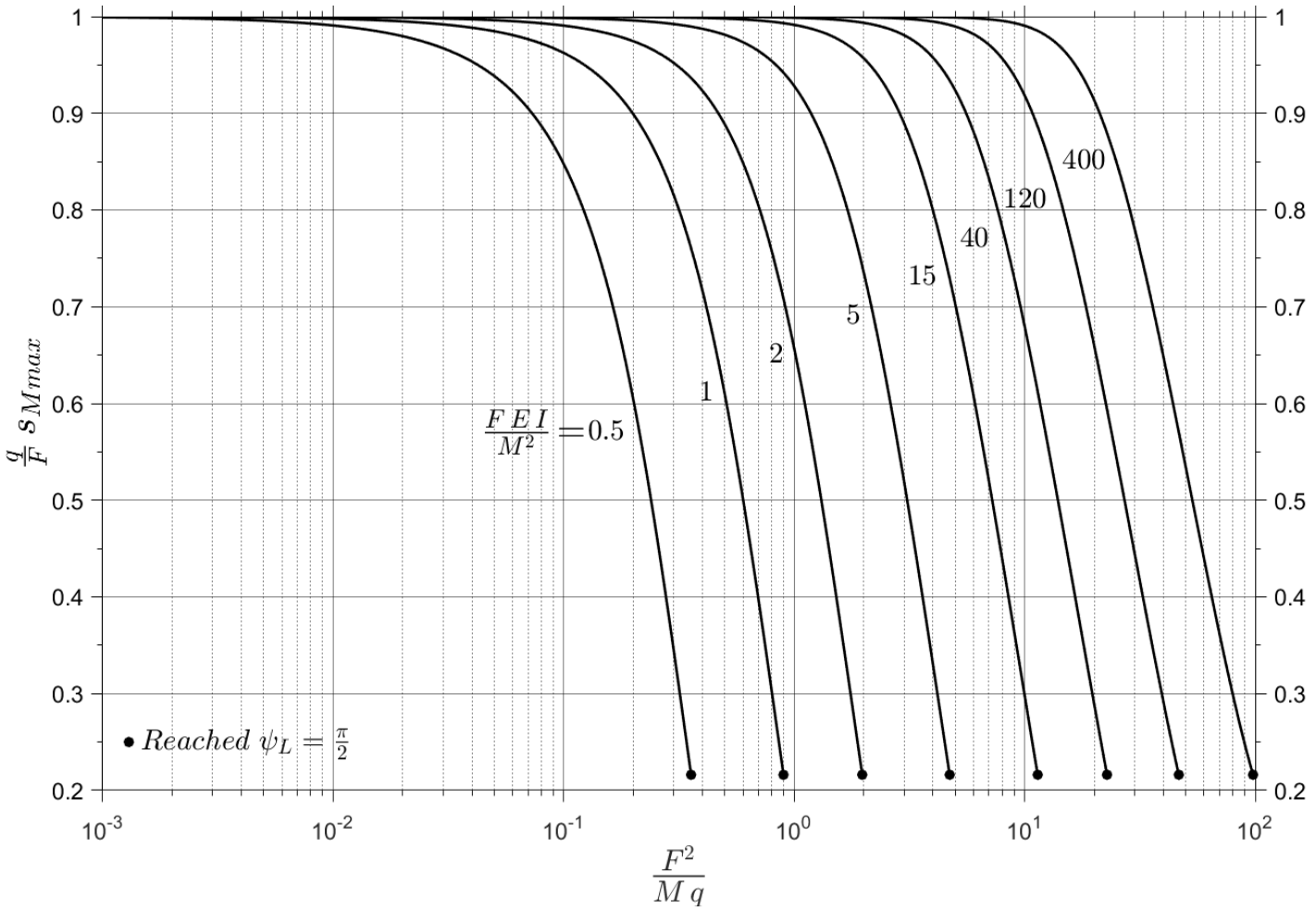


**Fig.10** Dimensionless curvilinear where bending moment reaches its maximum value - case $M > 0$

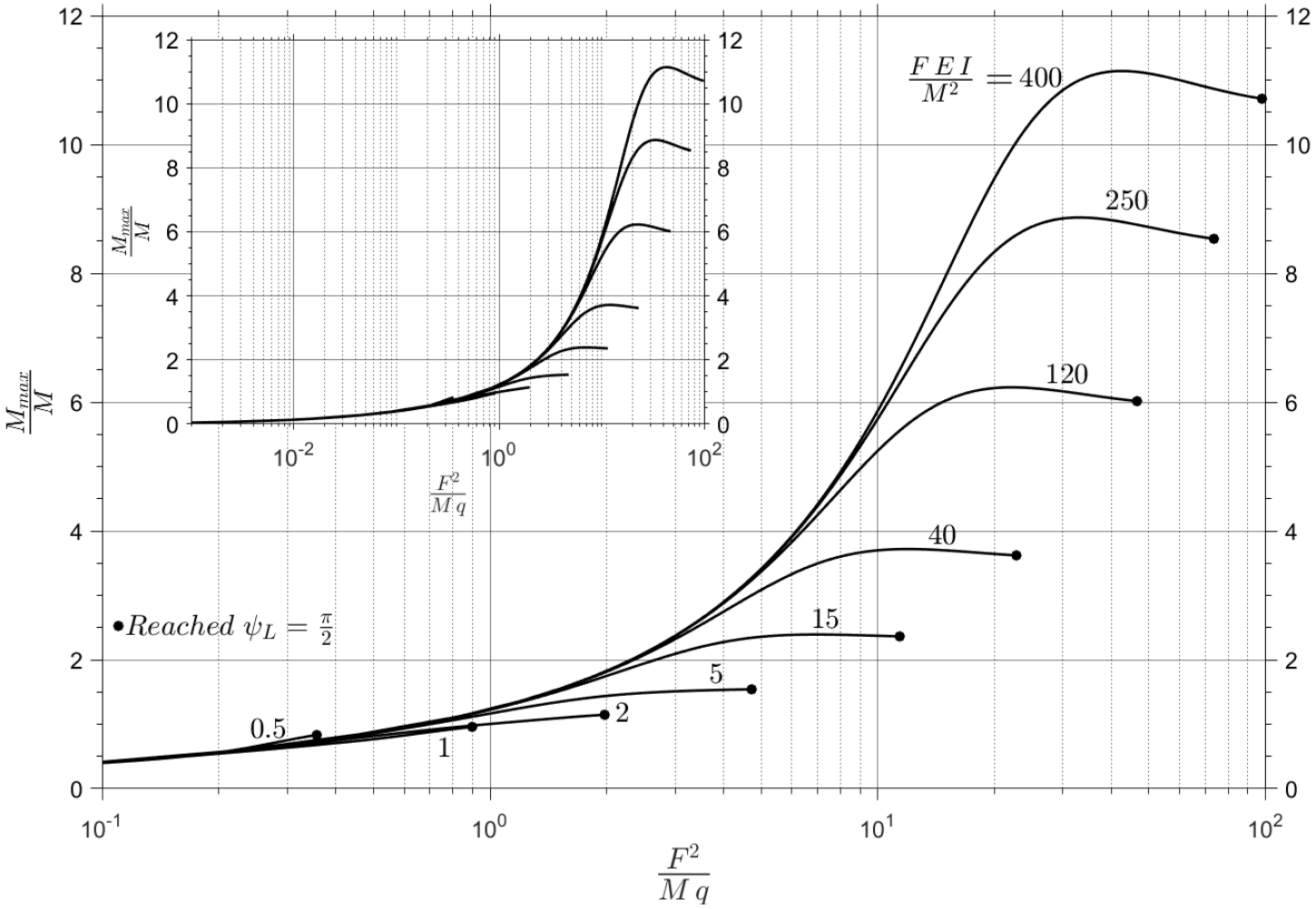


**Fig.11** Dimensionless maximum bending moment - case $M > 0$

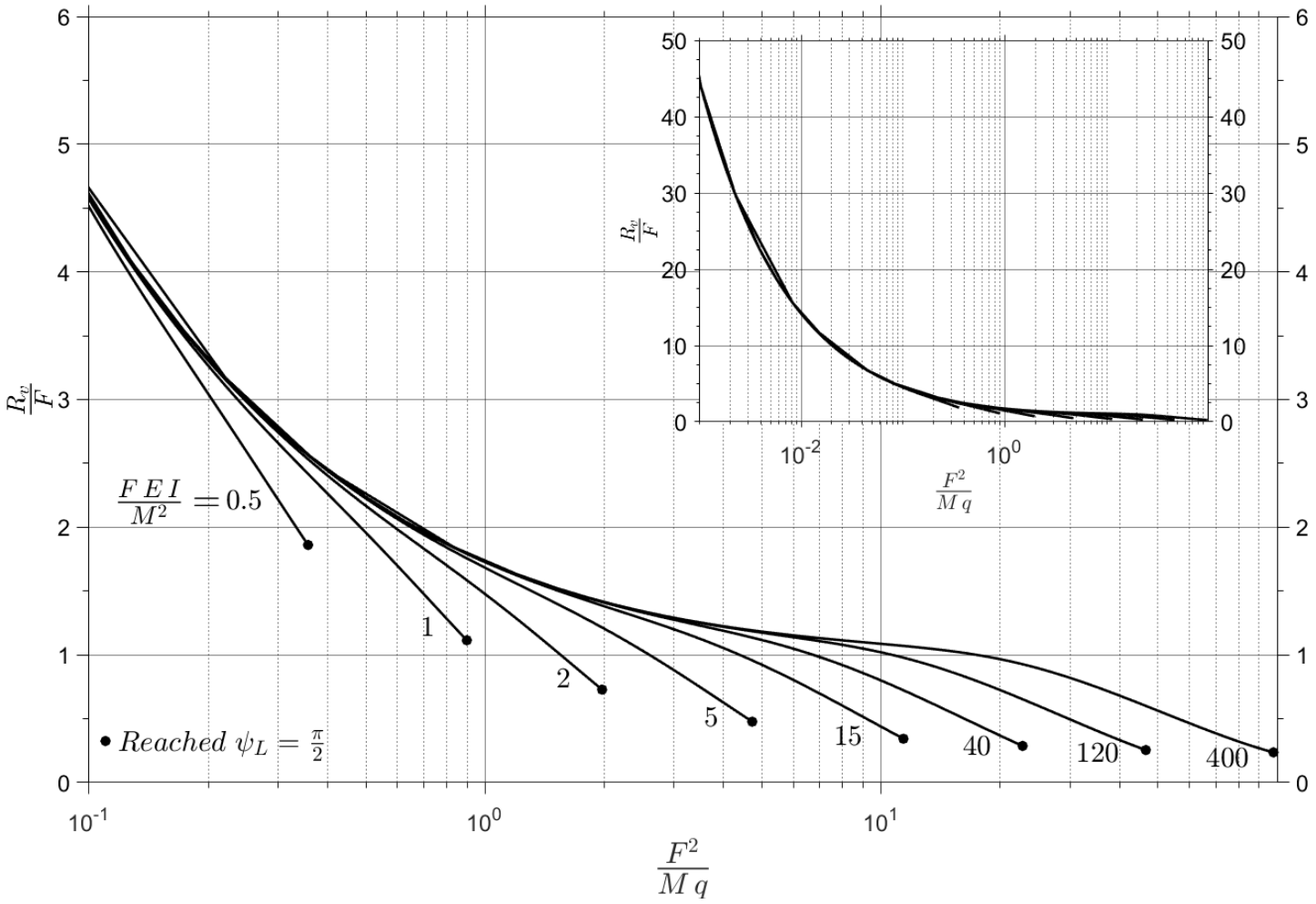


**Fig.12** Dimensionless constrain-reaction force - case $M > 0$

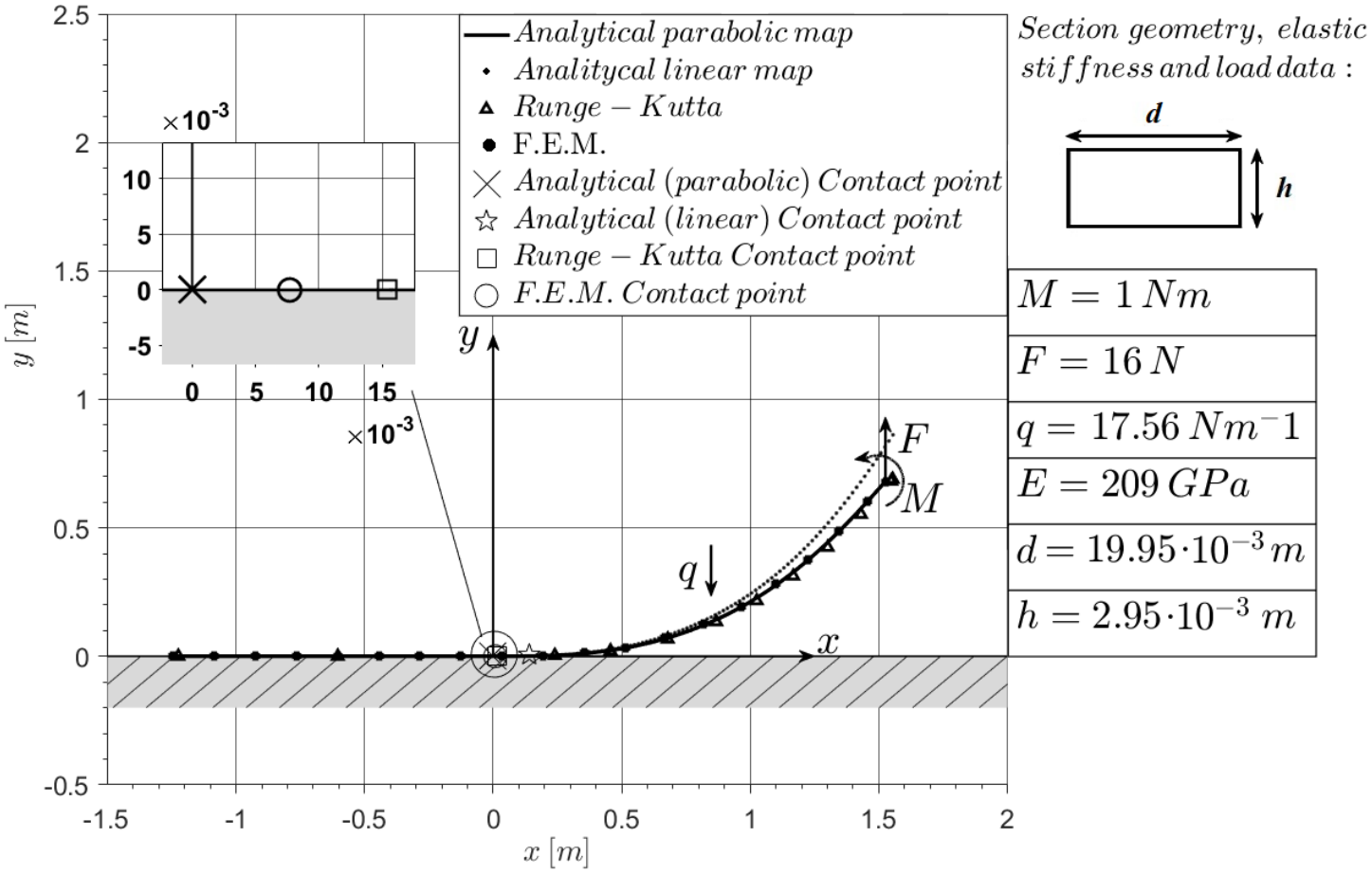


**Fig.13** Displacement configuration according to Analytical parabolic map, Analytical linear map, Runge-Kutta and F.E.M results

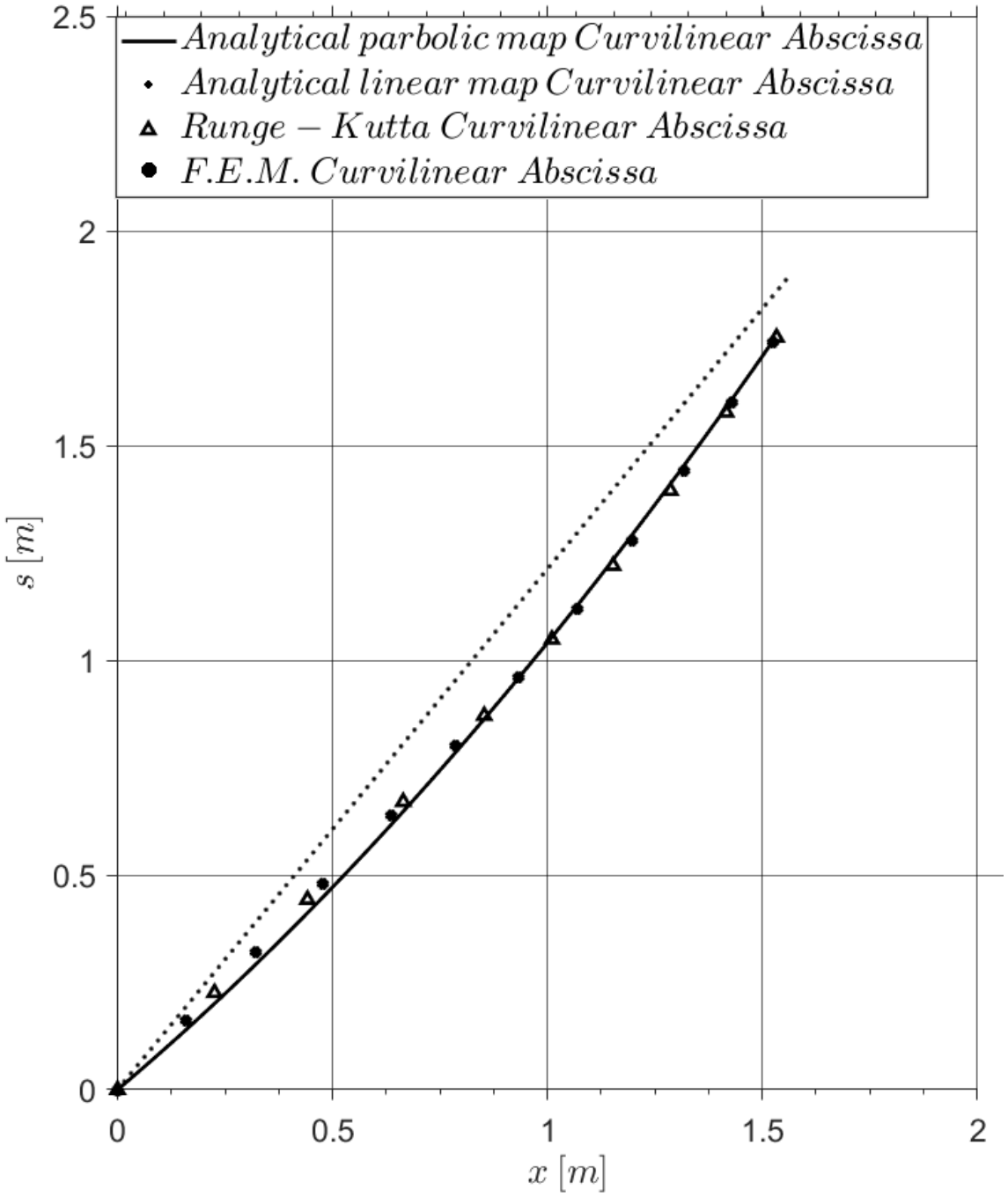


**Fig.14** Curvilinear abscissa versus x Cartesian coordinate according to Analytical parabolic map, Analytical linear map, Runge-Kutta and F.E.M results

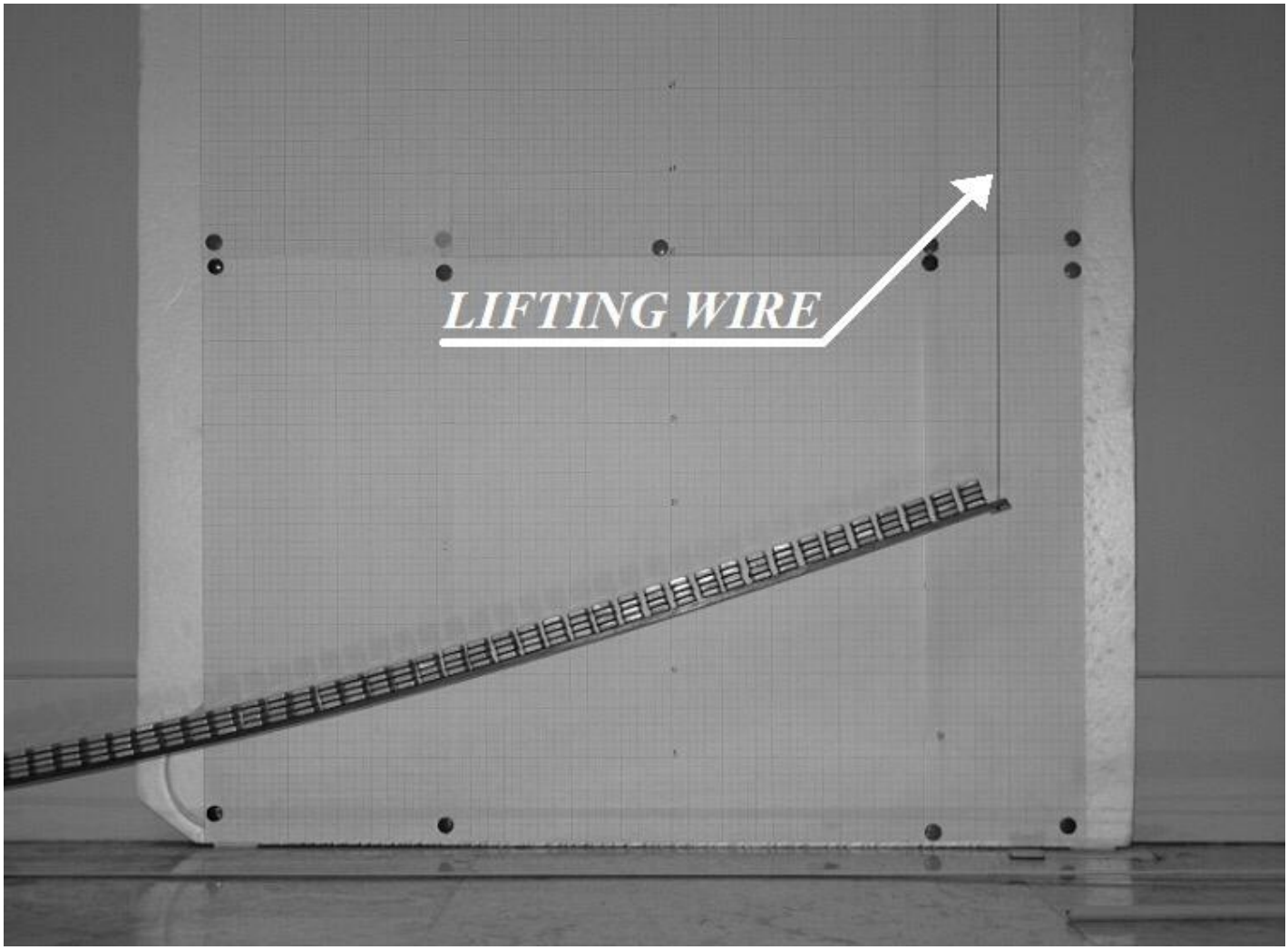


**Fig.15** Experimental test. Lifting wire when four weights are piled

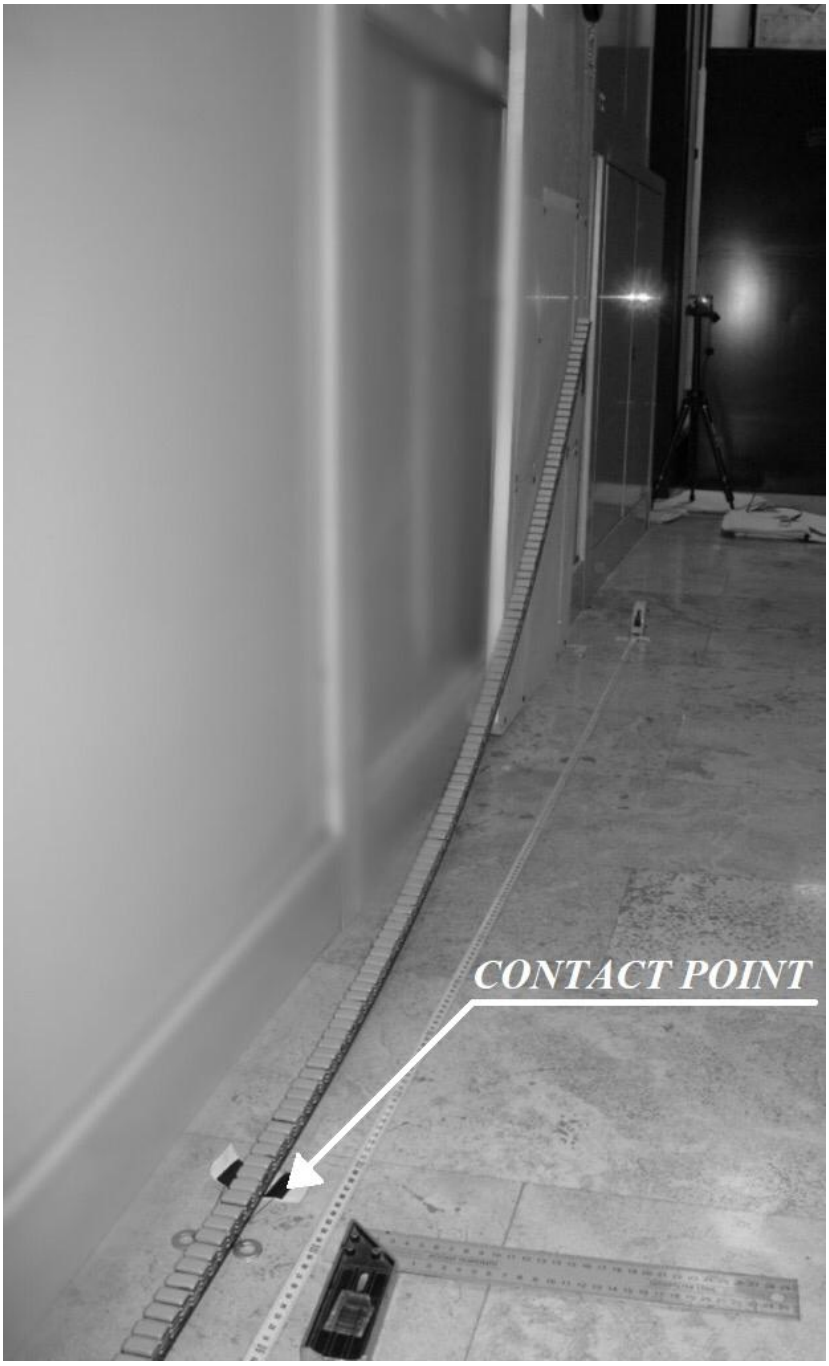


**Fig.16** Experimental test. Contact point identification

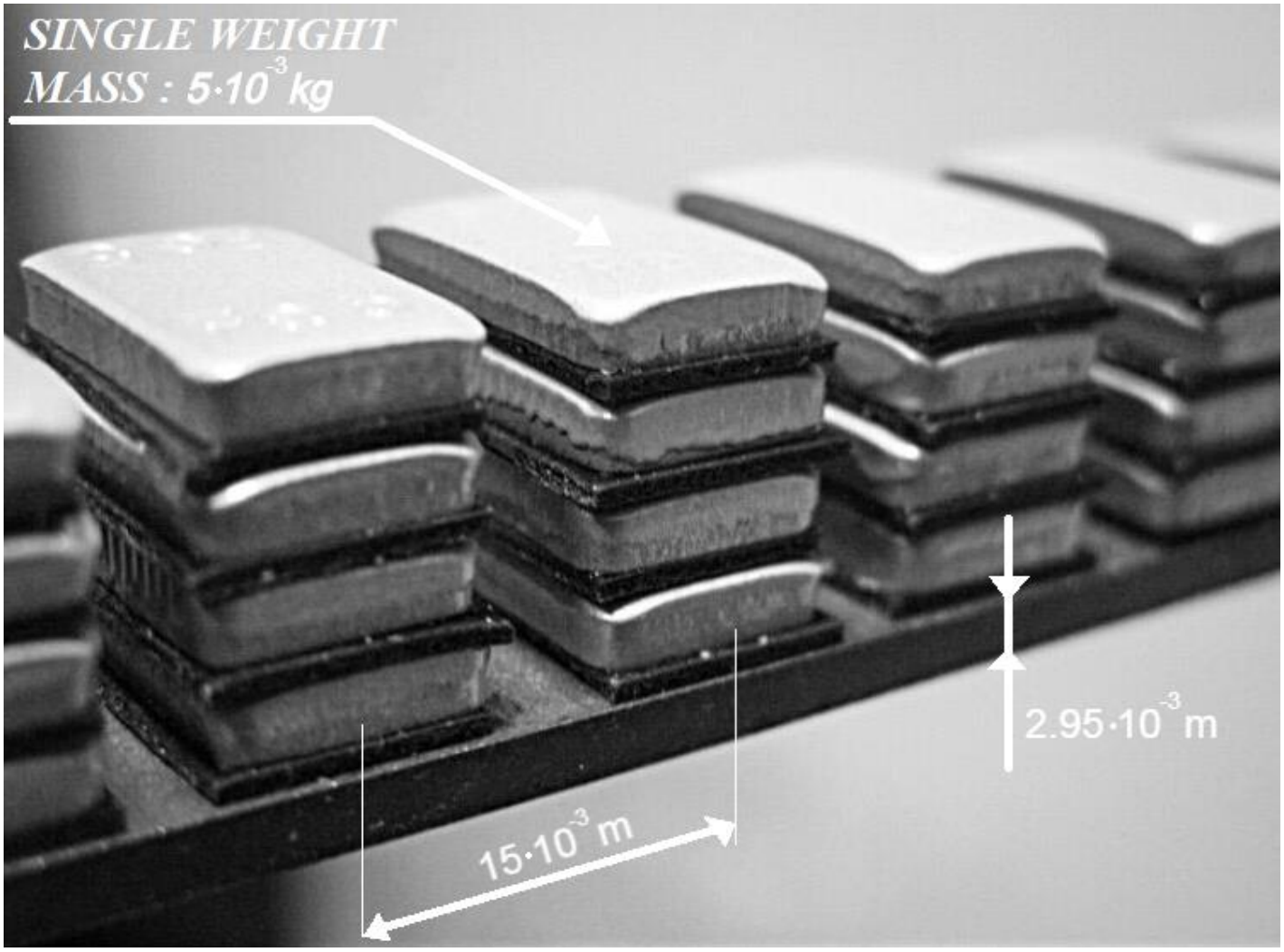


**Fig.17** Experimental test. Piling of the additional weights

**Table 1** Vertical displacement $y_L$ and percentage difference according to different methods

| $\lvert\Delta_{y_L}\ \%\rvert$ | Analytical parabolic map | Analytical linear map | Runge-Kutta | F.E.M. |
|---|---|---|---|---|
| Analytical parabolic map | 0 | *26.54* | *0.08* | *0.01* |
| Analytical linear map | *SYM* | 0 | *26.44* | *26.67* |
| Runge-Kutta | | | 0 | *0.18* |
| F.E.M. | | | | 0 |
| **Vertical displ.$y_L$ [mm]** | **680.96** | **861.71** | **681.52** | **680.29** |
| **End angle $\psi_L$ [deg]** | **48.77** | **56.66** | **48.90** | **48.83** |

**Table 2** Experimental and numerical results: self-weight load $q$=4.482 $Nm^{-1}$

| **Vertical Dis-placement** | **Experimental data – Average values** | | | **Analytical** | | | **Runge-Kutta** | | |
|---|---|---|---|---|---|---|---|---|---|
| | $F$ $[N]$ | $L_{tot}-L$ [mm] | $\psi_L$ [deg] | $F$ $[N]$ | $L_{tot}-L$ [mm] | $\psi_L$ [deg] | $F$ $[N]$ | $L_{tot}-L$ [mm] | $\psi_L$ [deg] |
| $y_L = 200\ mm$ | **3.943** | *1037.6* | 13,30 | **3.973** | *1023.8* | 13.01 | **3.973** | *1024.0* | 13.01 |
| $y_L = 400\ mm$ | **4.905** | *717.8* | 22,20 | 4.807 | *707.6* | 21.92 | 4.807 | *708.7* | 21.91 |
| $y_L = 600\ mm$ | **5.454** | *397.0* | 30,40 | **5.435** | *409.1* | 29.65 | **5.435** | *409.6* | 29.61 |

**Table 3** Experimental and numerical results: one weight added $q$=7.752 $Nm^{-1}$

| Vertical Displacement | Experimental data – Average values | | | Analytical | | | Runge-Kutta | | |
|---|---|---|---|---|---|---|---|---|---|
| | $F$ $[N]$ | $L_{tot}-L$ [mm] | $\psi_L$ [deg] | $F$ $[N]$ | $L_{tot}-L$ [mm] | $\psi_L$ [deg] | $F$ $[N]$ | $L_{tot}-L$ [mm] | $\psi_L$ [deg] |
| $y_L = 200\ mm$ | **5.906** | *1205.3* | 14, 80 | **6.013** | *1226.2* | 14.95 | **6.013** | *1226.4* | 14.94 |
| $y_L = 400\ mm$ | **7.220** | *940.5* | 25, 50 | **7.308** | *951.6* | 25.12 | **7.308** | *953.7* | 25.09 |
| $y_L = 600\ mm$ | **8.397** | *707.3* | 34, 10 | **8.329** | *686.7* | 34.01 | **8.328** | *686.8* | 33.95 |

**Table 4** Experimental and numerical results: two weights piled $q$=11.022 $Nm^{-1}$

| Vertical Displacement | Experimental data – Average values | | | Analytical | | | Runge-Kutta | | |
|---|---|---|---|---|---|---|---|---|---|
| | $F$ $[N]$ | $L_{tot}-L$ [mm] | $\psi_L$ [deg] | $F$ $[N]$ | $L_{tot}-L$ [mm] | $\psi_L$ [deg] | $F$ $[N]$ | $L_{tot}-L$ [mm] | $\psi_L$ [deg] |
| $y_L = 200\ mm$ | **7.711** | *126.8* | 16, 20 | **7.848** | *129.8* | 16.33 | **7.848** | *129.9* | 16.32 |
| $y_L = 400\ mm$ | **9.470** | *106.7* | 27, 20 | **9.584** | *105.4* | 27.46 | **9.584** | *105.6* | 27.42 |
| $y_L = 600\ mm$ | **10.918** | *78.8* | 37, 40 | **10.987** | *80.1* | 37.15 | **10.987** | *79.9* | 37.06 |

**Table 5** Experimental and numerical results: three weights piled $q$=14.292 $Nm^{-1}$

| Vertical Displacement | Experimental data – Average values | | | Analytical | | | Runge-Kutta | | |
|---|---|---|---|---|---|---|---|---|---|
| | $F$ $[N]$ | $L_{tot}-L$ [mm] | $\psi_L$ [deg] | $F$ $[N]$ | $L_{tot}-L$ [mm] | $\psi_L$ [deg] | $F$ $[N]$ | $L_{tot}-L$ [mm] | $\psi_L$ [deg] |
| $y_L = 200\ mm$ | 9.241 | *137.7* | 17,60 | 9.565 | *138.2* | 17.47 | 9.565 | *138.2* | 17.46 |
| $y_L = 400\ mm$ | 11.330 | *116.5* | 29,90 | 11.703 | *115.4* | 29.23 | 11.703 | *115.4* | 29.19 |
| $y_L = 600\ mm$ | 13.126 | *96.4* | 39,80 | 13.489 | *94.9* | 39.56 | 13.489 | *95.0* | 39.46 |

**Table 6** Experimental evidence and numerical results: four weights piled $q$=17.562 $Nm^{-1}$

| Vertical Displacement | Experimental data – Average values | | | Analytical | | | Runge-Kutta | | |
|---|---|---|---|---|---|---|---|---|---|
| | $F$ $[N]$ | $L_{tot}-L$ [mm] | $\psi_L$ [deg] | $F$ $[N]$ | $L_{tot}-L$ [mm] | $\psi_L$ [deg] | $F$ $[N]$ | $L_{tot}-L$ [mm] | $\psi_L$ [deg] |
| $y_L = 200\ mm$ | 10.869 | *141.7* | 18,50 | 11.164 | *144.7* | 18.31 | 11.164 | *144.8* | 18.30 |
| $y_L = 400\ mm$ | 13.175 | *120.6* | 30,70 | 13.734 | *118.7* | 30.80 | 13.734 | *118.6* | 30.75 |
| $y_L = 600\ mm$ | 15.352 | *104.7* | 41,50 | 15.902 | *102.9* | 41.63 | 15.902 | *102.9* | 41.52 |